Disturbance Rejection Control With Voltage Constraint for Electro-Hydraulic System Involving Unknown Dead-Zones and Drastic Supply Pressure Variation

Shengfei Liu, Liwu Wang, Chun Li, Qinglin Sun, Zenqiang Chen, Mingwei Sun, Xianyi Zeng

IEEE Access
Multidisciplinary ⋮ Rapid Review ⋮ Open Access Journal

Received April 9, 2020, accepted April 25, 2020, date of publication April 29, 2020, date of current version May 18, 2020.

Digital Object Identifier 10.1109/ACCESS.2020.2991162

Disturbance Rejection Control With Voltage Constraint for Electro-Hydraulic System Involving Unknown Dead-Zones and Drastic Supply Pressure Variation

SHENGFEI LIU[1], LIWU WANG[2], CHUN LI[2], QINGLIN SUN[1], ZENGQIANG CHEN[1], MINGWEI SUN[1], AND XIANYI ZENG[3], (Senior Member, IEEE)

[1]College of Artificial Intelligence, Nankai University, Tianjin 300350, China
[2]Beijing Institute of Space Mechanics and Electricity, Beijing 100094, China
[3]Gemtex Laboratory, Ecole Nationale Supérieure des Arts et Industries Textiles, 59100 Roubaix, France

Corresponding author: Qinglin Sun (sunql@nankai.edu.cn)

This work was supported in part by the National Natural Science Foundation of China under Grant 61973172, Grant 61273138, Grant 61973175, and Grant 61573197, in part by the Key Technologies Research and Development Program of Tianjin under Grant 19JCZDJC32800, in part by the Science and Technology Program of Tianjin under Grant 15ZXGTSF00020, and in part by the Open Funding of the Beijing Institute of Space Mechanics and Electricity.

ABSTRACT In the article, we use the proportional directional valve (PDV) with unknown dead-zones to regulate the electro-hydraulic system (EHS) which has parametric uncertainties including the drastic supply pressure variation; moreover, the external disturbance occurs when the EHS works; in addition, the control voltage applied to the PDV is expected to satisfy the prescribed bound. All of these factors make controller design a challenging problem. The unknown dead-zones, the external disturbance, the drastic supply pressure variation and other parametric uncertainties are viewed as a total disturbance which can be estimated by the linear extended state observer (LESO). Furthermore, a novel robust disturbance rejection position controller with voltage constraints is proposed to compensate for the dead-zones and improve the tracking performance of the EHS regulated by the PDV when the drastic supply pressure variation and the external disturbance occur. The stability analysis is given to ensure that the tracking error of the closed-loop EHS regulated by the proposed controller can converge to the arbitrarily small neighborhood of the origin. Experiments are carried out to verify the effectiveness of the proposed control method. Comparative experimental results demonstrate that the proposed controller can make the load follow the reference trajectory accurately in the presence of the unknown dead-zones and the external disturbance when the supply pressure varies drastically.

INDEX TERMS Disturbance rejection control, electro-hydraulic system, voltage constraint, unknown dead-zones, drastic supply pressure variation, linear extended state observer, proportional directional valve.

I. INTRODUCTION

The electro-hydraulic systems (EHS) play a very important role in a wide variety of applications, such as robots [1], heavy engineering machineries [2], fatigue test device [3] and load simulators [4] due to high-response, large power-to-weight ratios and the ability to generate large actuation force [5]. Although the servo valve can be used to regulate the flow rate of the hydraulic oil, it is expensive and prone to malfunction resulting from fluid contamination [6]. To reduce manufacturing cost and sensitivity to contamination [7], [8], the proportional directional valve (PDV) is widely utilized in the EHS. The main difference between the servo valve and the PDV is that the servo valve has no dead-zones [9], but the PDV has dead-zones due to overlaps between the spool and the sleeve [10]. The dead-zones degrade the tracking performance when the expected direction of the motion changes [8]. Moreover, the control voltage applied to the PDV is required to satisfy the prescribed voltage range in order that the PDV can be protected from being damaged.

A direct dead-zone compensation method based on a describing function was put forward for the EHS regulated

The associate editor coordinating the review of this manuscript and approving it for publication was Jianyong Yao.

by the PDV with known symmetric dead-zones [11]. However, there may exist asymmetric dead-zones in the PDV [12]. Moreover, it is difficult and expensive to measure the exact width of dead-zones in the PDV. By selecting a Lyapunov-Krasovskii functional, an adaptive compensation controller was designed to handle unknown asymmetric dead-zones [13]. A nonlinear robust adaptive controller based on the smooth dead-zone inverse was designed to compensate for the unknown valve dead-zone [14].

There are parametric uncertainties in many practical control systems; a robust fault-tolerant H_∞ controller was proposed to handle parametric uncertainty in the offshore steel jacket platform system [15]. In addition, some parameters in the EHS are time-varying [16], [17]. For example, the effective bulk modulus of the hydraulic oil alters because of the entrained air [18]. Internal leakage coefficient varies due to component wear and the change of the oil viscosity which alters with the oil temperature; the discharge coefficient of the orifice changes with the variation of the Reynolds number of the oil [19]. To tackle parametric uncertainties, a discontinuous projection-based adaptive control law was used in [20]. However, in [20], the servo valve was adopted to regulate the flow rate of the hydraulic oil and the actuator was a double-rod hydraulic cylinder, in which ram areas of two chambers were equal, but we use the PDV to adjust the flow rate of the oil and the actuator in our test setup is a single-rod hydraulic cylinder, in which ram areas of two chambers are not equal. Different ram areas make the controller design more difficult.

Furthermore, the supply pressure fluctuation may occur in the practical EHS. The feedback linearization method was used to compensate for the supply pressure variation in the EHS regulated by the servo valve [18]. The actuator in [18] was a hydraulic motor whereas the actuator in our test platform is a hydraulic cylinder. As far as we know, rather few research work has been carried out to design the controller which can compensate for the drastic supply pressure variation in the practical EHS controlled by the PDV. Therefore, it is necessary to conduct the research in order that the tracking performance of the EHS regulated by the PDV can be improved when the supply pressure drops drastically.

Moreover, disturbances exist in the EHS due to the unknown varying external load [21], [22], the nonlinear frictions [23], and other unmodeled dynamics [24]. Disturbance observers are widely adopted to estimate the disturbance since it is difficult to measure the disturbance in the EHS. A second-order high-pass filter was used to develop a disturbance observer such that a biased sinusoidal disturbance can be estimated [25]. By using the high-gain disturbance observer and the barrier Lyapunov fucntion, a backstepping controller was designed to compensate for the disturbance and restrict the tracking error in a prescribed bound [26]. A T-S state fuzzy observer was used to estimate the vehicle side-slip angle and a dissipative fault-tolerant fuzzy controller was put forward to attenuate the disturbance in the vehicle lateral motion control systems [27].

In practical control systems, the control input is expected to satisfy the prescribed bounds due to physical input saturation on hardware [28]–[30]. A Nussbaum function was adopted to tackle the control saturation of the servo valve in [21], but the PDV is used in our test setup for the EHS, where the control voltage applied to the PDV is required to locate in $[-10\text{ V}, 10\text{ V}]$; otherwise, the PDV will be damaged.

Main contributions of the article are: we use the linear extended state observer (LESO) to estimate the total disturbance which includes the unknown dead-zones, the external disturbance and the drastic supply pressure variation; furthermore, a novel controller is designed to compensate for the total disturbance effectively; the performance of disturbance rejection is improved; the robustness for drastic supply pressure variation is enhanced; to satisfy voltage constraints on the PDV, the control voltage is restricted in $[-10\text{ V}, 10\text{ V}]$ such that the PDV can be protected from being damaged; the analysis on tracking error is provided to ensure that the tracking error can converge to the arbitrarily small neighborhood of the origin.

The article is arranged as follows. In section II, the mathematical model of the electro-hydraulic system regulated by the PDV is described; in section III, a novel extended state observer based controller with constrained voltage is designed; furthermore, in section IV, the estimation error analysis is given to ensure that the total disturbance can be estimated accurately; the tracking error analysis is conducted to guarantee that the load can follow the reference trajectory precisely; to verify the performance of the proposed controller, comparative experiments are carried out in section V; eventually, the conclusion is presented in section VI.

II. MATHEMATICAL MODEL OF ELECTRO-HYDRAULIC SYSTEM REGULATED BY PDV

The schematic diagram of a single-rod electro-hydraulic system is illustrated in Figure 1. Firstly, the oil is drawn from the oil tank by the pump driven by the electric motor. After that, it flows into the PDV through the check valve. The flow rate and direction of the oil can be changed by adjusting the control voltage applied to the solenoid of the PDV; the oil flows into the cylinder across the PDV so that the piston can drive the load to move.

According to Newton's second law, the dynamics of the load can be described by

$$m\ddot{y} = P_1A_1 - P_2A_2 - b\dot{y} - sgn(\dot{y})f_1 + f_2. \tag{1}$$

where m is mass of the load; y is displacement of the load; P_1 is pressure inside the rod side chamber; P_2 is pressure inside the cap side chamber; A_1 is ram area of the rod side; A_2 is ram area of the cap side; b is the damping coefficient between the piston and cylinder; sgn is the sign function; f_1 is the sliding friction force between the load and the rail, $f_1 = \mu mg$, μ is the sliding friction coefficient, g is gravitational acceleration; f_2 is the unmodeled dynamics which includes the unmodeled nonlinear friction forces and other hard-to-model terms [24].

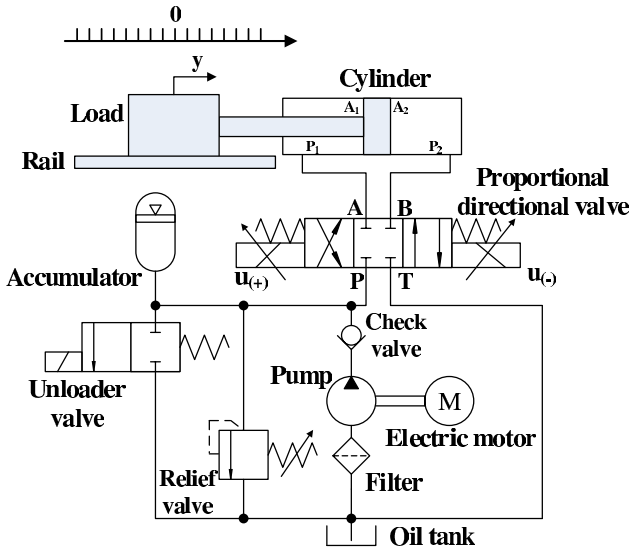

FIGURE 1. Electro-hydraulic system regulated by proportional directional valve.

In the article, the pressures of two chambers can be measured by pressure sensors so that the thrust of the cylinder can be calculated by

$$F(t) = P_1(t)A_1 - P_2(t)A_2. \tag{2}$$

To make the description clear, the following assumptions are given:

In Figure 1, if the load stays on the right side of the origin, the displacement of the load is positive; if the load stays on the left side of the origin, the displacement of the load is negative; if the load moves right, the velocity of the load is positive; if the load moves left, the velocity of the load is negative; if the direction of the thrust is right, the thrust is positive; if the direction of the thrust is left, the thrust is negative.

The cylinder dynamics [19] is given by

$$\begin{cases} \frac{V_1}{\beta_e}\dot{P}_1 = -A_1\dot{y} - C_{ip}(P_1 - P_2) \\ \qquad\qquad -C_{em1}(P_1 - P_T) + Q_1, \\ \frac{V_2}{\beta_e}\dot{P}_2 = A_2\dot{y} + C_{ip}(P_1 - P_2) \\ \qquad\qquad -C_{em2}(P_2 - P_T) - Q_2. \end{cases} \tag{3}$$

where V_1 is total control volume of the rod side chamber; V_2 is total control volume of the cap side chamber; β_e is effective bulk modulus of the hydraulic oil; C_{ip} is coefficient of the internal leakage of the cylinder; C_{em1} and C_{em2} denote coefficients of the external leakage of the chamber; P_T is oil tank pressure; Q_1 is the flow rate to the rod side chamber; Q_2 is the flow rate of the cap side chamber. V_1 and V_2 can be given by

$$V_1 = V_{01} + A_1 y, V_2 = V_{02} - A_2 y. \tag{4}$$

where V_{01} and V_{02} are two chamber volumes when $y = 0$. With the improvement of seal techniques, the external leakage of the cylinder is neglected. Therefore, $C_{em1} = 0$, $C_{em2} = 0$, so that we obtain

$$\begin{cases} \dot{P}_1 = -\frac{A_1\beta_e}{V_1}\dot{y} - \frac{C_{ip}\beta_e}{V_1}(P_1 - P_2) + \frac{\beta_e}{V_1}Q_1, \\ \dot{P}_2 = \frac{A_2\beta_e}{V_2}\dot{y} + \frac{C_{ip}\beta_e}{V_2}(P_1 - P_2) - \frac{\beta_e}{V_2}Q_2. \end{cases} \tag{5}$$

A three-land-four-way proportional directional valve (PDV) is used to adjust the flow rate and direction of the oil in the paper. The relationship between the oil flow rate and the orifice opening is given by [19], [31] as follows

$$Q_1 = \begin{cases} C_d w x_{nv}\sqrt{\frac{2}{\rho}|P_S - P_1|}, & x_{nv} \geq 0, \\ C_d w x_{nv}\sqrt{\frac{2}{\rho}|P_1 - P_T|}, & x_{nv} < 0. \end{cases} \tag{6}$$

$$Q_2 = \begin{cases} C_d w x_{nv}\sqrt{\frac{2}{\rho}|P_2 - P_T|}, & x_{nv} \geq 0, \\ C_d w x_{nv}\sqrt{\frac{2}{\rho}|P_S - P_2|}, & x_{nv} < 0. \end{cases} \tag{7}$$

where C_d is coefficient of discharge of the PDV orifice; w is area gradient of the PDV orifice; x_{nv} is the orifice opening of the PDV; ρ is oil density; P_S is the supply pressure which equals the pressure of the pump.

Let $k_q = C_d w\sqrt{\frac{2}{\rho}}$, $P_3 = |P_S - P_1|$, $P_4 = |P_1 - P_T|$, $P_5 = |P_2 - P_T|$, $P_6 = |P_S - P_2|$, we can define

$$\sigma_1(*) = \begin{cases} 1, & * \geq 0 \\ 0, & * < 0 \end{cases} \tag{8}$$

Furthermore, we can obtain

$$\begin{cases} Q_1 = k_q x_{nv}\left[\sigma_1(x_{nv})\sqrt{P_3} + \sigma_1(-x_{nv})\sqrt{P_4}\right], \\ Q_2 = k_q x_{nv}\left[\sigma_1(x_{nv})\sqrt{P_5} + \sigma_1(-x_{nv})\sqrt{P_6}\right] \end{cases} \tag{9}$$

From (9), it can be seen that the flow and direction of the hydraulic oil can be changed by adjusting the orifice opening of the PDV. Moreover, the relationship between the orifice opening and the spool displacement can be given by

$$x_{nv} = \begin{cases} x_v - d_1, & x_v > d_1 \\ 0, & -d_2 \leq x_v \leq d_1 \\ x_v + d_2, & x_v < -d_2 \end{cases} \tag{10}$$

where x_v is the spool displacement of the PDV, $x_v = k_0 u$, u is the control voltage applied to the PDV, k_0 is the gain of the PDV; d_1 and d_2 are the dead-zone widths for the negative and positive spool displacement, respectively. The simplified structure of the PDV is described in Fig.2 where it can be seen that the PDV has a quite large dead-zone because the width of the land is greater than that of the port in the valve sleeve when the spool of the PDV is at neutral [11], [19], [32]. Consequently, the oil flow is zero when $-d_2 \leq x_v \leq d_1$.

Furthermore, we can calculate x_{nv} by

$$x_{nv} = \sigma_2(u) = \begin{cases} k_0 u - d_1, & u > \frac{d_1}{k_0} \\ 0, & -\frac{d_2}{k_0} \leq u \leq \frac{d_1}{k_0} \\ k_0 u + d_2, & u < -\frac{d_2}{k_0} \end{cases} \tag{11}$$

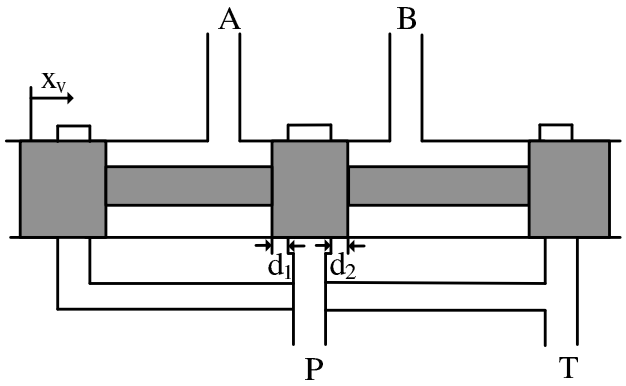

FIGURE 2. The simplified structure of the PDV.

From (11), it can be seen that the orifice opening is zero when $-\frac{d_2}{k_0} \le u \le \frac{d_1}{k_0}$. The flow rate of the rod side chamber and that of the cap side chamber are zero when the orifice opening is zero according to (9). Hence, the load will keep motionless when $-\frac{d_2}{k_0} \le u \le \frac{d_1}{k_0}$. From the aforementioned analysis, the relationship between the control voltage and the displacement of the load in the single-rod electro-hydraulic system can be described by

$$\ddot{y} = \frac{A_1}{m}P_1 - \frac{A_2}{m}P_2 - \frac{b}{m}\dot{y} - sgn(\dot{y})\mu g + \frac{f_2}{m} \tag{12}$$

and

$$\begin{cases} \dot{P}_1 = & -\dfrac{A_1\beta_e}{V_{01}+A_1 y}\dot{y} - \dfrac{C_{ip}\beta_e}{V_{01}+A_1 y}(P_1 - P_2) \\ & +\dfrac{\beta_e}{V_{01}+A_1 y}Q_1, \\ \dot{P}_2 = & \dfrac{A_2\beta_e}{V_{02}-A_2 y}\dot{y} + \dfrac{C_{ip}\beta_e}{V_{02}-A_2 y}(P_1 - P_2) \\ & -\dfrac{\beta_e}{V_{02}-A_2 y}Q_2, \\ Q_1 = & k_q\sigma_2(u)\left[\sigma_3(u)\sqrt{P_3} + \sigma_4(u)\sqrt{P_4}\right], \\ Q_2 = & k_q\sigma_2(u)\left[\sigma_3(u)\sqrt{P_5} + \sigma_4(u)\sqrt{P_6}\right] \end{cases} \tag{13}$$

where $\sigma_3(u) = \sigma_1(\sigma_2(u))$, $\sigma_4(u) = \sigma_1(-\sigma_2(u))$.

III. POSITION TRACKING CONTROLLER DESIGN

A. DISTURBANCE ESTIMATION

Extended state observer (ESO) was put forward by Han [33]–[35]. With the help of ESO, the nonlinearities and the uncertainties can be regarded as the total disturbance which can be compensated for by the controller [36]–[38]. The ESO can be linearized so that the linear extended state observer (LESO) can be obtained. Furthermore, the observer bandwidth is given to make it easier to tune the parameters of LESO by Gao [39]. An adaptive controller combined with the ESO was proposed to suppress the unmodeled disturbances for a servo-valve controlled electro-hydraulic system with a double-rod hydraulic cylinder in [40]. In addition, the ESO can be applied to estimate the additive disturbance and the system states which are difficult to measure [41]. There are dead-zone, nonlinear friction, and unmodeled dynamics in the electro-hydraulic system regulated by the proportional directional valve. These factors make it difficult to control the position of the load accurately. However, these factors can be regarded as the total disturbance. Because the control voltage and the load position can be measured, the LESO can estimate the total disturbance in the electro-hydraulic system exactly. Furthermore, with the help of the information given by the LESO, the controller can be designed to compensate for the disturbance so that the load can follow the reference trajectory precisely. From the aforementioned analysis, it can be concluded that the load position can be changed by adjusting the control voltage applied to the PDV. However, the control voltage is not included explicitly in (12). Fortunately, there are several terms related with the control voltage in (12). By adjusting the control voltage, the flow of the hydraulic oil is altered, with the result that the velocity of the piston varies. Consequently, the velocity of the load alters. Therefore, those terms, encompassing $\dot{y}$ in (12), will change when the oil flow varies. Furthermore, they are related with the control voltage. Hence, we obtain:

$$-sgn(\dot{y})\mu g - \frac{b}{m}\dot{y} = b_1 u \tag{14}$$

where b_1 is the gain of the control voltage, $b_1 \neq 0$ and it can be tuned according to the control performance. Combining (14) with (12), we obtain:

$$\begin{aligned} \ddot{y} &= \frac{1}{m}(P_1A_1 - P_2A_2) + \frac{f_2}{m} + b_1 u \\ &= \frac{1}{m}(P_1A_1 - P_2A_2) + \frac{f_2}{m} + (b_1 - b_0)u + b_0 u \end{aligned} \tag{15}$$

where b_0 is the estimation of b_1, $b_0 \approx b_1$; moreover, to compare the disturbance rejection performance of the different controllers, the external disturbance is added to the control signal so that we have

$$u = u_1 + w_1 \tag{16}$$

where u_1 is the output of the controller and w_1 is the external disturbance. As a result, the disturbance rejection performance of the different controllers can be tested when w_1 takes various disturbance signals. Furthermore, substituting (16) into (15), we obtain

$$\begin{aligned} \ddot{y} = &\frac{1}{m}(P_1A_1 - P_2A_2) + \frac{f_2}{m} + b_0 w_1 \\ &+(b_1 - b_0)(u_1 + w_1) + b_0 u_1 \end{aligned} \tag{17}$$

Let

$$\begin{aligned} f = &\frac{1}{m}(P_1A_1 - P_2A_2) + \frac{f_2}{m} + b_0 w_1 \\ &+(b_1 - b_0)(u_1 + w_1) \end{aligned} \tag{18}$$

Combining (17) with (18), we obtain

$$\ddot{y} = f + b_0 u_1 \tag{19}$$

where f is the total disturbance which includes the internal disturbance, the external disturbance and the unmodeled dynamics. The total disturbance f can be regarded as the

extended state. Let $x_1 = y, x_2 = \dot{y}, x_3 = f$ so that (19) can be written as

$$\begin{cases} \dot{x}_1 = x_2 \\ \dot{x}_2 = x_3 + b_0 u_1 \\ \dot{x}_3 = h \\ y = x_1 \end{cases} \tag{20}$$

where x_3 is the extended state, $h = \dot{f}$. Furthermore, (20) can be written in the matrix form

$$\begin{cases} \dot{x} = Ax + Bu_1 + Eh \\ y = Cx \end{cases} \tag{21}$$

where $x = \begin{bmatrix} x_1 \\ x_2 \\ x_3 \end{bmatrix}, A = \begin{bmatrix} 0 & 1 & 0 \\ 0 & 0 & 1 \\ 0 & 0 & 0 \end{bmatrix}, B = \begin{bmatrix} 0 \\ b_0 \\ 0 \end{bmatrix}, E = \begin{bmatrix} 0 \\ 0 \\ 1 \end{bmatrix}$, $C = \begin{bmatrix} 1 & 0 & 0 \end{bmatrix}$. The LESO for system (21) is given by

$$\begin{cases} \dot{\hat{x}} = A\hat{x} + Bu_1 + L(y - \hat{y}) \\ \hat{y} = C\hat{x} \end{cases} \tag{22}$$

where $\hat{x}$ is the estimate of the state x, $\hat{x} = \begin{bmatrix} \hat{x}_1 & \hat{x}_2 & \hat{x}_3 \end{bmatrix}^T$, $\hat{y}$ is the estimate of the load position, L is the observer gain matrix, $L = \begin{bmatrix} L_1 & L_2 & L_3 \end{bmatrix}^T$. To obtain L, we need to calculate the estimation error by

$$\varepsilon(t) = x(t) - \hat{x}(t) \tag{23}$$

where $\varepsilon(t)$ is the estimation error of the state, and $\varepsilon(t) = \begin{bmatrix} \varepsilon_1(t) & \varepsilon_2(t) & \varepsilon_3(t) \end{bmatrix}^T$. Taking the time-derivative of the estimation error, we have

$$\dot{\varepsilon}(t) = \dot{x}(t) - \dot{\hat{x}}(t) \tag{24}$$

Combining (21), (22) with (24), we obtain

$$\dot{\varepsilon}(t) = (A - LC)\varepsilon(t) + Eh(t) \tag{25}$$

where $h(t)$ is the time-derivative of the total disturbance,

$$A - LC = \begin{bmatrix} -L_1 & 1 & 0 \\ -L_2 & 0 & 1 \\ -L_3 & 0 & 0 \end{bmatrix}.$$

The characteristic polynomial of $A - LC$ is given by

$$\det(\lambda I - (A - LC)) = \lambda^3 + L_1\lambda^2 + L_2\lambda + L_3 \tag{26}$$

All eigenvalues of $A - LC$ are placed in $-\omega_o$ ($\omega_o > 0$) to ensure that the LESO is bounded-input bounded-output stable when $h(t)$ is bounded [39]; ω_o denotes the bandwidth of the observer. Therefore, the observer gain L can be determined by

$$\begin{aligned} \lambda^3 + L_1\lambda^2 + L_2\lambda + L_3 = (\lambda + \omega_o)^3 = \lambda^3 + 3\omega_o\lambda^2 \\ +3\omega_o^2\lambda + \omega_o^3 \end{aligned} \tag{27}$$

which yields

$$L = \begin{bmatrix} L_1 \\ L_2 \\ L_3 \end{bmatrix} = \begin{bmatrix} 3\omega_o \\ 3\omega_o^2 \\ \omega_o^3 \end{bmatrix}. \tag{28}$$

B. DESIGNING A DISTURBANCE-REJECTION CONTROLLER WITH BOUNDED CONTROL VOLTAGE

In order to suppress external disturbances and internal disturbances including dead-zone of the valve, parameter uncertainties and meanwhile keep the control voltage in the prescribed range, we propose a novel disturbance-rejection controller as

$$u_1 = \frac{1}{b_0}(k_1\varphi(z_1) + k_2\varphi(z_2) - \hat{x}_3 + \ddot{r}) \tag{29}$$

where

$$\begin{cases} \varphi(z_i) & = \dfrac{z_i}{\sqrt{1 + z_i^2}}, i = 1, 2 \\ z_1 & = k_3\xi_1 + k_4\xi_2 \\ z_2 & = k_4\xi_2 \\ \xi_1 & = r - y \\ \xi_2 & = \dot{\xi}_1 \end{cases} \tag{30}$$

where $k_j > 0, j = 1, 2, 3, 4$; r is the reference signal; $\hat{x}_3$ is the estimate of the total disturbance; ξ_1 is the tracking error; ξ_2 is the time derivative of the tracking error. The closed-loop electro-hydraulic system regulated by the proposed controller is illustrated in Fig.3, where D denotes the differentiation operator.

Remark 1: It is assumed that the second order derivative of the reference signal is bounded. Moreover, the estimate of the total disturbance is bounded since the real disturbance is bounded and the estimation error of the total disturbance is bounded, which will be proven in the subsequent section. Furthermore, the external disturbance w_1 is bounded and $|\varphi(z_i)| \leq 1, i = 1, 2$. Hence, b_0 can be chosen to ensure that u can satisfy the prescribed range of the control voltage which is [−10 V, 10 V] for the PDV in our test setup.

Remark 2: Although it is very difficult to measure the exact real value of the total disturbance in the practical electro-hydraulic system regulated by the proportional directional valve, we can calculate the estimate of the total disturbance with the help of LESO given by (22); furthermore, we design a disturbance compensation term $\hat{x}_3$ in the proposed controller u_1 described in (29) such that the total disturbance can be compensated for effectively.

IV. STABILITY ANALYSIS AND BOUND OF CONTROL INPUT

To guarantee that the electro-hydraulic system can track the expected trajectory accurately, the stability analysis is necessary [42]. Therefore, we conduct a thorough stability analysis for the electro-hydraulic system. Firstly, we make an analysis for the estimation error of the linear extended state observer because the total disturbance can not be measured and moreover, the proposed controller depends on the estimated total disturbance. Next, we conduct the tracking error analysis to ensure that the closed-loop electro-hydraulic system can track the reference trajectory accurately and the tracking error can converge to the arbitrarily small neighborhood of the origin.

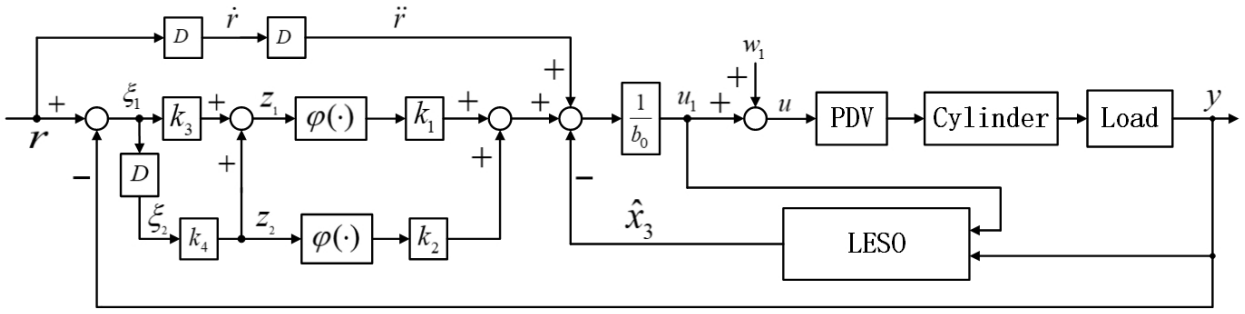

FIGURE 3. Block diagram of the closed-loop electro-hydraulic position control system regulated by the proposed controller.

A. ESTIMATION ERROR ANALYSIS

From (22), we obtain

$$\begin{bmatrix}\dot{\hat{x}}_1\\ \dot{\hat{x}}_2\\ \dot{\hat{x}}_3\end{bmatrix}=\begin{bmatrix}0&1&0\\0&0&1\\0&0&0\end{bmatrix}\begin{bmatrix}\hat{x}_1\\ \hat{x}_2\\ \hat{x}_3\end{bmatrix}+\begin{bmatrix}0\\ b_0\\ 0\end{bmatrix}u_1+L\left(y-\hat{x}_1\right). \tag{31}$$

Combining (28) with (31), we obtain

$$\begin{cases}\dot{\hat{x}}_1=\hat{x}_2+L_1\left(x_1-\hat{x}_1\right)\\ \dot{\hat{x}}_2=\hat{x}_3+L_2\left(x_1-\hat{x}_1\right)+b_0u_1\\ \dot{\hat{x}}_3=L_3\left(x_1-\hat{x}_1\right)\end{cases} \tag{32}$$

Furthermore, we have

$$\begin{cases}\dot{\varepsilon}_1=\dot{x}_1-\dot{\hat{x}}_1\\ \dot{\varepsilon}_2=\dot{x}_2-\dot{\hat{x}}_2\\ \dot{\varepsilon}_3=\dot{x}_3-\dot{\hat{x}}_3\end{cases} \tag{33}$$

Combining (20), (32) with (33), we obtain

$$\begin{cases}\dot{\varepsilon}_1=-L_1\varepsilon_1+\varepsilon_2\\ \dot{\varepsilon}_2=-L_2\varepsilon_1+\varepsilon_3\\ \dot{\varepsilon}_3=-L_3\varepsilon_1+h\end{cases} \tag{34}$$

Let $\delta_i(t)=\frac{\varepsilon_i(t)}{\omega_o^{i-1}},\ i=1,\ 2,\ 3$, then we obtain

$$\begin{cases}\dot{\delta}_1=-L_1\delta_1+\omega_o\delta_2\\ \dot{\delta}_2=-\dfrac{L_2}{\omega_o}\delta_1+\omega_o\delta_3\\ \dot{\delta}_3=-\dfrac{L_3}{\omega_o^2}\delta_1+\dfrac{h}{\omega_o^2}\end{cases} \tag{35}$$

Furthermore, (35) can be written in the matrix form as follows:

$$\dot{\delta}(t)=\omega_oA_\delta\delta(t)\ +B_\delta\frac{h(t)}{\omega_o^2}. \tag{36}$$

where $\delta(t)=\begin{bmatrix}\delta_1(t)\\ \delta_2(t)\\ \delta_3(t)\end{bmatrix}, A_\delta=\begin{bmatrix}-3&1&0\\-3&0&1\\-1&0&0\end{bmatrix}, B_\delta=\begin{bmatrix}0\\0\\1\end{bmatrix}$.

Theorem 1: If $|h(t)|\le H(H>0)$, then there exist Γ_i ($\Gamma_i>0,\ i=1,\ 2,\ 3$), and a definite time T_1 ($T_1>0$), such that $|\varepsilon_i(t)|\le\Gamma_i$ when $t>T_1$; Γ_i is related with ω_o, and $\frac{d\Gamma_i}{d\omega_o}<0$.

Proof: The solution of (36) is given by

$$\delta(t)=\exp(\omega_oA_\delta t)\delta(0)+q(t) \tag{37}$$

where

$$q(t)=\int_0^t\exp[\omega_oA_\delta(t-\tau)]B_\delta\frac{h(\tau)}{\omega_o^2}d\tau=\begin{bmatrix}q_1(t)\\ q_2(t)\\ q_3(t)\end{bmatrix} \tag{38}$$

The eigenvalues of ω_oA_δ are $-\omega_o,-\omega_o,-\omega_o$, because the eigenvalues of A_δ are $-1,-1,-1$. Hence, we have

$$\begin{aligned}\exp[\omega_oA_\delta(t-\tau)]&=e^{-\omega_o(t-\tau)}\sum_{k=0}^{2}\frac{(t-\tau)^k}{k!}\omega_o^kG_\delta^k\\&=e^{-\omega_o(t-\tau)}\begin{bmatrix}\Lambda_{11}&\Lambda_{12}&\Lambda_{13}\\ \Lambda_{21}&\Lambda_{22}&\Lambda_{23}\\ \Lambda_{31}&\Lambda_{32}&\Lambda_{33}\end{bmatrix}\end{aligned} \tag{39}$$

where $G_\delta=A_\delta+I, I=\begin{bmatrix}1&0&0\\0&1&0\\0&0&1\end{bmatrix}$, and

$$\begin{cases}\Lambda_{11}=1-2(t-\tau)\omega_o+\dfrac{(t-\tau)^2}{2}\omega_o^2\\ \Lambda_{12}=(t-\tau)\omega_o-\dfrac{(t-\tau)^2}{2}\omega_o^2\\ \Lambda_{13}=\dfrac{(t-\tau)^2}{2}\omega_o^2\\ \Lambda_{21}=-3(t-\tau)\omega_o+(t-\tau)^2\omega_o^2\\ \Lambda_{22}=1+(t-\tau)\omega_o-(t-\tau)^2\omega_o^2\\ \Lambda_{23}=(t-\tau)\omega_o+(t-\tau)^2\omega_o^2\\ \Lambda_{31}=-(t-\tau)\omega_o+\dfrac{(t-\tau)^2}{2}\omega_o^2\\ \Lambda_{32}=-\dfrac{(t-\tau)^2}{2}\omega_o^2\\ \Lambda_{33}=1+(t-\tau)\omega_o+\dfrac{(t-\tau)^2}{2}\omega_o^2\end{cases} \tag{40}$$

Combining (38), (39), and (40), we obtain

$$\begin{cases}q_1(t)=\dfrac{1}{2}\displaystyle\int_0^t(t-\tau)^2e^{-\omega_o(t-\tau)}h(\tau)d\tau\\ q_2(t)=\dfrac{1}{\omega_o^2}\displaystyle\int_0^tp_1(\tau)e^{-\omega_o(t-\tau)}h(\tau)d\tau\\ q_3(t)=\dfrac{1}{\omega_o^2}\displaystyle\int_0^tp_2(\tau)e^{-\omega_o(t-\tau)}h(\tau)d\tau\end{cases} \tag{41}$$

where $p_1(\tau)=(t-\tau)\omega_o+(t-\tau)^2\omega_o^2$, and $p_2(\tau)=1+(t-\tau)\omega_o+\frac{(t-\tau)^2}{2}\omega_o^2$.

Since $h(\tau)$ is bounded, there exists H $(H > 0)$, $|h(\tau)| \leq H$. Therefore, when $t > 0$, we have

$$\begin{aligned} |q_1(t)| &= \frac{1}{2}\left|\int_0^t (t-\tau)^2 e^{-\omega_o(t-\tau)} h(\tau) d\tau\right| \\ &\leq \frac{1}{2}\int_0^t \left|(t-\tau)^2 e^{-\omega_o(t-\tau)} h(\tau)\right| d\tau \\ &\leq \frac{H}{2}\int_0^t (t-\tau)^2 e^{-\omega_o(t-\tau)} d\tau \\ &= \frac{H}{\omega_o^3}[1-(\frac{\omega_o^2}{2}t^2 e^{-\omega_o t} + \omega_o t e^{-\omega_o t} + e^{-\omega_o t})] \\ &< \frac{H}{\omega_o^3} \end{aligned} \tag{42}$$

Similarly, we have

$$\begin{cases} |q_2(t)| < \dfrac{3H}{\omega_o^3} \\ |q_3(t)| < \dfrac{3H}{\omega_o^3} \end{cases} \tag{43}$$

Since the eigenvalues of $\omega_o A_\delta$ are $-\omega_o, -\omega_o, -\omega_o$, we obtain

$$\begin{aligned} \exp(\omega_o A_\delta t) &= e^{-\omega_o t}\sum_{k=0}^{2}\frac{t^k}{k!}\omega_o^k (A_\delta + I)^k \\ &= e^{-\omega_o t}[I + t\omega_o(A_\delta + I) + \frac{t^2}{2}\omega_o^2 (A_\delta + I)^2] \\ &= \begin{bmatrix} c_{11} & c_{12} & c_{13} \\ c_{21} & c_{22} & c_{23} \\ c_{31} & c_{32} & c_{33} \end{bmatrix} \end{aligned} \tag{44}$$

where

$$\begin{cases} c_{11} = (1 - 2\omega_o t + \dfrac{\omega_o^2}{2}t^2)e^{-\omega_o t} \\ c_{12} = (\omega_o t - \dfrac{\omega_o^2}{2}t^2)e^{-\omega_o t} \\ c_{13} = \dfrac{\omega_o^2}{2}t^2 e^{-\omega_o t} \\ c_{21} = (-3\omega_o t + \omega_o^2 t^2)e^{-\omega_o t} \\ c_{22} = (1 + \omega_o t - \omega_o^2 t^2)e^{-\omega_o t} \\ c_{23} = (\omega_o t + \omega_o^2 t^2)e^{-\omega_o t} \\ c_{31} = (-\omega_o t + \dfrac{\omega_o^2}{2}t^2)e^{-\omega_o t} \\ c_{32} = -\dfrac{\omega_o^2}{2}t^2 e^{-\omega_o t} \\ c_{33} = (1 + \omega_o t + \dfrac{\omega_o^2}{2}t^2)e^{-\omega_o t} \end{cases} \tag{45}$$

Since $\lim_{t\to\infty} c_{ij}(t) = 0$, there exists T_1 $(T_1 > 0)$, when $t > T_1$, $\left|c_{ij}(t)\right| < \frac{1}{\omega_o^3}$, $i, j = 1, 2, 3$.

Moreover, combining (37), (38), with (44), we obtain

$$\begin{aligned} \delta(t) &= \begin{bmatrix} c_{11} & c_{12} & c_{13} \\ c_{21} & c_{22} & c_{23} \\ c_{31} & c_{32} & c_{33} \end{bmatrix}\begin{bmatrix} \delta_1(0) \\ \delta_2(0) \\ \delta_3(0) \end{bmatrix} + \begin{bmatrix} q_1(t) \\ q_2(t) \\ q_3(t) \end{bmatrix} \\ &= \begin{bmatrix} \delta_1(t) \\ \delta_2(t) \\ \delta_3(t) \end{bmatrix} \end{aligned} \tag{46}$$

Furthermore, when $t > T_1$, we have

$$\begin{aligned} |\delta_1(t)| &\leq |c_{11}(t)\delta_1(0)| + |c_{12}(t)\delta_2(0)| + |c_{13}(t)\delta_3(0)| \\ &\quad + |q_1(t)| \\ &\leq \frac{1}{\omega_o^3}(|\delta_1(0)| + |\delta_2(0)| + |\delta_3(0)| + H) \end{aligned} \tag{47}$$

Since $\delta_1(t) = \varepsilon_1(t), \delta_1(0) = \varepsilon_1(0), \delta_2(0) = \frac{\varepsilon_2(0)}{\omega_o}$, $\delta_3(0) = \frac{\varepsilon_3(0)}{\omega_o^2}$, we obtain

$$|\varepsilon_1(t)| \leq \frac{|\varepsilon_1(0)|}{\omega_o^3} + \frac{|\varepsilon_2(0)|}{\omega_o^4} + \frac{|\varepsilon_3(0)|}{\omega_o^5} + \frac{H}{\omega_o^3} = \Gamma_1$$

$$\frac{d\Gamma_1}{d\omega_o} = -\frac{3\,|\varepsilon_1(0)|}{\omega_o^4} - \frac{4\,|\varepsilon_2(0)|}{\omega_o^5} - \frac{5\,|\varepsilon_3(0)|}{\omega_o^6} - \frac{3H}{\omega_o^4} < 0 \tag{48}$$

Similarly, we have

$$|\varepsilon_2(t)| \leq \frac{|\varepsilon_1(0)|}{\omega_o^2} + \frac{|\varepsilon_2(0)|}{\omega_o^3} + \frac{|\varepsilon_3(0)|}{\omega_o^4} + \frac{3H}{\omega_o^2} = \Gamma_2$$

$$\frac{d\Gamma_2}{d\omega_o} = -\frac{2\,|\varepsilon_1(0)|}{\omega_o^3} - \frac{3\,|\varepsilon_2(0)|}{\omega_o^4} - \frac{4\,|\varepsilon_3(0)|}{\omega_o^5} - \frac{6H}{\omega_o^3} < 0 \tag{49}$$

$$|\varepsilon_3(t)| \leq \frac{|\varepsilon_1(0)|}{\omega_o} + \frac{|\varepsilon_2(0)|}{\omega_o^2} + \frac{|\varepsilon_3(0)|}{\omega_o^3} + \frac{3H}{\omega_o} = \Gamma_3$$

$$\frac{d\Gamma_3}{d\omega_o} = -\frac{|\varepsilon_1(0)|}{\omega_o^2} - \frac{2\,|\varepsilon_2(0)|}{\omega_o^3} - \frac{3\,|\varepsilon_3(0)|}{\omega_o^4} - \frac{3H}{\omega_o^2} < 0 \tag{50}$$

From the aforementioned analysis, it can be seen that when the derivative of the disturbance is bounded, the estimation error of the linear extended state observer is bounded [43]; the estimation error can be reduced by increasing the bandwidth of the ESO. The proof is complete. □

Remark 3: According to (48), (49) and (50), the upper bounds of the estimation errors can be tuned small enough when the bandwidth of the ESO is selected large enough such that the total disturbance can be accurately estimated to meet the practical requirement.

B. ANALYSIS ON TRACKING ERROR

Theorem 2: If $|h(t)| \leq H(H > 0)$, then for any $\eta(\eta > 0)$, there exist $\Gamma_4(\Gamma_4 > 0)$ and $T_1(T_1 > 0)$, such that when $t > T_1$, $\|\xi\| \leq \eta$, where $\xi = \begin{bmatrix}\xi_1 & \xi_2\end{bmatrix}^T$ and $\|\xi\| = \sqrt{\xi_1^2 + \xi_2^2}$.

Proof: Combining (19) with (30), we have

$$\begin{cases} \dot{\xi}_1 = \xi_2 \\ \dot{\xi}_2 = \ddot{r} - x_3 - b_0 u_1 \end{cases} \tag{51}$$

Substituting (29) into (51), we obtain

$$\begin{aligned} \dot{\xi}_2 &= \ddot{r} - x_3 - k_1\varphi(z_1) - k_2\varphi(z_2) + \hat{x}_3 - \ddot{r} \\ &= -k_1\varphi(z_1) - k_2\varphi(z_2) - x_3 + \hat{x}_3 \end{aligned} \tag{52}$$

Furthermore, we have

$$\begin{cases} \dot{\xi}_1 = \xi_2 \\ \dot{\xi}_2 = -k_1\varphi(z_1) - k_2\varphi(z_2) - \tilde{x}_3 \end{cases} \tag{53}$$

where $\tilde{x}_3$ is the estimation error of the total disturbance and $\tilde{x}_3 = x_3 - \hat{x}_3$. Lyapunov function can be selected as

$$V = k_1(\sqrt{1 + z_1^2} - 1) + k_2(\sqrt{1 + z_2^2} - 1) + \frac{1}{2}k_3\xi_2^2 \tag{54}$$

Taking time derivative, we have

$$\begin{aligned}\dot{V} &= k_1\frac{z_1}{\sqrt{1+z_1^2}}\dot{z}_1 + k_2\frac{z_2}{\sqrt{1+z_2^2}}\dot{z}_2 + k_3\xi_2\dot{\xi}_2 \\ &= k_1\varphi(z_1)(k_3\dot{\xi}_1 + k_4\dot{\xi}_2) + k_2k_4\varphi(z_2)\dot{\xi}_2 + k_3\xi_2\dot{\xi}_2 \end{aligned} \tag{55}$$

Let

$$\begin{cases}\rho_1 = \varphi(z_1) \\ \rho_2 = \varphi(z_2) + \frac{\tilde{x}_3}{k_2}\end{cases} \tag{56}$$

We have

$$\begin{aligned}\dot{\xi}_2 &= -k_1\varphi(z_1) - k_2\varphi(z_2) - [k_2\rho_2 - k_2\varphi(z_2)] \\ &= -k_1\varphi(z_1) - k_2\varphi(z_2) - k_2\rho_2 + k_2\varphi(z_2) \\ &= -k_1\rho_1 - k_2\rho_2 \end{aligned} \tag{57}$$

Substituting (56) and (57) into (55), we obtain

$$\begin{aligned}\dot{V} &= k_1(k_3\xi_2 + k_4(-k_1\rho_1 - k_2\rho_2))\rho_1 \\ &\quad +k_2k_4\dot{\xi}_2(\rho_2 - \frac{\tilde{x}_3}{k_2}) + k_3\xi_2\dot{\xi}_2 \\ &= k_1\rho_1(k_3\xi_2 - k_1k_4\rho_1 - k_2k_4\rho_2) \\ &\quad +k_2k_4\dot{\xi}_2\rho_2 - k_4\dot{\xi}_2\tilde{x}_3 + k_3\xi_2\dot{\xi}_2 \\ &= k_1k_3\rho_1\xi_2 - k_1^2k_4\rho_1^2 - k_1k_2k_4\rho_1\rho_2 \\ &\quad +k_2k_4\rho_2(-k_1\rho_1 - k_2\rho_2) - k_4\dot{\xi}_2\tilde{x}_3 \\ &\quad +k_3\xi_2(-k_1\rho_1 - k_2\rho_2) \\ &= k_1k_3\rho_1\xi_2 - k_1^2k_4\rho_1^2 - k_1k_2k_4\rho_1\rho_2 \\ &\quad -k_1k_2k_4\rho_1\rho_2 - k_2^2k_4\rho_2^2 - k_4\dot{\xi}_2\tilde{x}_3 \\ &\quad -k_1k_3\rho_1\xi_2 - k_2k_3\xi_2\rho_2 \\ &= -k_1^2k_4\rho_1^2 - 2k_1k_2k_4\rho_1\rho_2 \\ &\quad -k_2^2k_4\rho_2^2 - k_4\dot{\xi}_2\tilde{x}_3 - k_2k_3\xi_2\rho_2 \\ &= -k_4(k_1^2\rho_1^2 + 2k_1k_2\rho_1\rho_2 + k_2^2\rho_2^2) \\ &\quad -k_4\dot{\xi}_2\tilde{x}_3 - k_2k_3\xi_2\rho_2 \\ &= -k_4(k_1\rho_1 + k_2\rho_2)^2 - k_4\dot{\xi}_2\tilde{x}_3 - k_2k_3\xi_2\rho_2 \\ &= -k_4(k_1\varphi(z_1) + k_2\varphi(z_2) + \tilde{x}_3)^2 \\ &\quad +k_4(k_1\varphi(z_1) + k_2\varphi(z_2) + \tilde{x}_3)\tilde{x}_3 \\ &\quad -k_2k_3\xi_2\varphi(z_2) - k_3\xi_2\tilde{x}_3 \\ &= -k_4[(k_1\varphi(z_1) + k_2\varphi(z_2) + \tilde{x}_3)^2 \\ &\quad -(k_1\varphi(z_1) + k_2\varphi(z_2) + \tilde{x}_3)\tilde{x}_3] \\ &\quad -k_2k_3\xi_2\varphi(z_2) - k_3\xi_2\tilde{x}_3 \end{aligned} \tag{58}$$

Let $\rho_3 = k_1\varphi(z_1) + k_2\varphi(z_2)$ so that we can obtain

$$\begin{aligned}\dot{V} &= -k_4[(\rho_3 + \tilde{x}_3)^2 - (\rho_3 + \tilde{x}_3)\tilde{x}_3] \\ &\quad -k_2k_3\xi_2\varphi(z_2) - k_3\xi_2\tilde{x}_3 \\ &= -k_4\rho_3(\rho_3 + \tilde{x}_3) - k_2k_3\xi_2\varphi(z_2) \\ &\quad -k_3\xi_2\tilde{x}_3 \\ &\le -k_4\rho_3(\rho_3 + \tilde{x}_3) - k_2k_3\xi_2\varphi(z_2) \\ &\quad +k_3\left|\xi_2\right|\left|\tilde{x}_3\right| \\ &= -k_4\rho_3(\rho_3 + \tilde{x}_3) - (k_2k_3\xi_2\varphi(z_2) \\ &\quad -k_3\left|\xi_2\right|\left|\tilde{x}_3\right|) \end{aligned} \tag{59}$$

Since $|h(t)| \le H$, according to Theorem 1, there exist $T_1(T_1 > 0)$ and $\Gamma_3(\Gamma_3 > 0)$, when $t > T_1$, $|\tilde{x}_3| \le \Gamma_3$; in addition, $\xi_2\varphi(z_2) = \frac{k_4\xi_2^2}{\sqrt{1+k_4^2\xi_2^2}} > 0$ (when $\xi_2 \ne 0$). Hence, when $t > T_1$, it is reasonable to select k_2 large enough such that

$$k_2k_3\xi_2\varphi(z_2) - k_3\left|\xi_2\right|\left|\tilde{x}_3\right| \ge 0 \tag{60}$$

Moreover, for any $\eta(\eta > 0)$, there exist η_1 and η_2, such that $\eta = \sqrt{\eta_1^2 + \eta_2^2}$. Futhermore, we can obtain Γ_4 by

$$\Gamma_4 = \left|\frac{k_1(k_3\eta_1 + k_4\eta_2)}{\sqrt{1+(k_3\eta_1 + k_4\eta_2)^2}} + \frac{k_2k_4\eta_2}{\sqrt{1+k_4^2\eta_2^2}}\right| \tag{61}$$

Combining (59) with (60), we know that $\dot{V} < 0$ if $t > T_1$ and $\|\xi\| > \eta$, since in this case, $|\rho_3| > \Gamma_4$; furthermore, according to (50), ω_o can be adjusted large enough such that $\Gamma_3 < \Gamma_4$; hence, $|\rho_3| > \Gamma_3$ which leads to $\rho_3(\rho_3 + \tilde{x}_3) > 0$ because $-\Gamma_3 \le \tilde{x}_3 \le \Gamma_3$ when $t > T_1$ according to Theorem 1. As a result, V decreases such that $\|\xi\| \le \eta$. The proof is complete. □

Remark 4: From Theorem 2, we can find that (ξ_1, ξ_2) will stay within the neighborhood of the origin with radius η, when $t > T_1$. Furthermore, we can select η to be an arbitrarily small positive number since Γ_3 can be made arbitrarily small by tuning ω_o large enough according to Theorem 1. Consequently, the tracking error and its time derivative can converge to the arbitrarily small neighborhood of the origin.

C. BOUND OF CONTROL INPUT

In this section, we will prove that the control voltage applied to the proportional directional valve can satisfy the prescribed range. From Theorem 1, we know that there exists a positive real number Γ_3, such that $\left|x_3 - \hat{x}_3\right| \le \Gamma_3$. Since $\left|\hat{x}_3\right| - |x_3| \le \left|\hat{x}_3 - x_3\right|$, we have

$$\left|\hat{x}_3\right| \le \Gamma_3 + |x_3| \tag{62}$$

where x_3 is the total disturbance, which is bounded in the practical electro-hydraulic system. Let $|x_3| \le \Gamma_5(\Gamma_5 > 0)$, where Γ_5 is the upper bound of x_3. Hence, $\left|\hat{x}_3\right| \le \Gamma_3 + \Gamma_5$. Let $\Gamma_3 + \Gamma_5 = \beta_1$, we obtain $\left|\hat{x}_3\right| \le \beta_1$. Similarly, $\ddot{r}$ and w_1 are bounded in the practical electro-hydraulic system. Therefore, $|\ddot{r}| \le \beta_2(\beta_2 > 0)$, $|w_1| \le \beta_3(\beta_3 > 0)$, where β_2 and β_3 are upper bounds of $\ddot{r}$ and w_1, respectively. Moreover, we assume that $\beta_3 < 10$. The following theorem can be obtained:

Theorem 3: If $b_0 \ge \frac{k_1+k_2+\beta_1+\beta_2}{10-\beta_3}$, then -10 V$\le u \le 10$ V, where k_1 and k_2 are gains of the proposed controller.

Proof: Combining (16) and (29) with (30), we have

$$\begin{aligned}|u| &= |u_1 + w_1| \le |u_1| + |w_1| \\ &= \left|\frac{1}{b_0}(k_1\varphi(z_1) + k_2\varphi(z_2) - \hat{x}_3 + \ddot{r})\right| + |w_1| \\ &= \frac{1}{b_0}\left|k_1\varphi(z_1) + k_2\varphi(z_2) - \hat{x}_3 + \ddot{r}\right| + |w_1| \\ &\le \frac{1}{b_0}(k_1\left|\varphi(z_1)\right| + k_2\left|\varphi(z_2)\right| + \left|\hat{x}_3\right| + |\ddot{r}|) + |w_1| \end{aligned}$$

$$= \frac{1}{b_0}(k_1\left|\frac{z_1}{\sqrt{1+z_1^2}}\right| + k_2\left|\frac{z_2}{\sqrt{1+z_2^2}}\right| + |\hat{x}_3| + |\ddot{r}|) + |w_1|$$
$$\leq \frac{1}{b_0}(k_1 + k_2 + |\hat{x}_3| + |\ddot{r}|) + |w_1| \quad (63)$$

Furthermore, we have

$$|u| \leq \frac{1}{b_0}(k_1 + k_2 + \beta_1 + \beta_2) + \beta_3 \quad (64)$$

Since $b_0 \geq \frac{k_1+k_2+\beta_1+\beta_2}{10-\beta_3}$, we obtain

$$|u| \leq \frac{10-\beta_3}{k_1+k_2+\beta_1+\beta_2}(k_1 + k_2 + \beta_1 + \beta_2) + \beta_3 = 10\ V \quad (65)$$

The proof is complete. □

V. EXPERIMENTAL VALIDATIONS

The experiment is conducted to validate the performance of the proposed controller in the test setup illustrated in Fig.4. The experimental platform is comprised of a proportional directional valve (Bosch Rexroth, 4WREE6E08-2X/G24K31/A1V, the maximum flow rate is 80 L/min; the maximum pressure is 315 bar; the maximum current is 2 A; the prescribed control voltage is [−10 V, 10 V]), a load (the mass is 3.97 kg), a gear pump (the pressure is 5 MPa), an AC motor to drive the pump, a single-rod cylinder (the external diameter and stroke are 40 mm, 200 mm, respectively; the diameters of the piston and the rod are 32 mm, 16 mm, respectively), a displacement sensor (MIRAN KTC-300) to measure the position of the load, 3 pressure transducers (ifm PT5402) to measure P_1, P_2, and P_S, respectively, a computer (the CPU frequency is 2.5 GHz; the memory size is 8 GB) to calculate the control signal applied to the proportional directional valve, and a 16-bit data acquisition board (ART Technology, USB3120, the sampling rate is 250 ksps) to receive the position information of the load and send the control signal to the proportional directional valve. The control program, running in the experiment platform, is written in C++ and compiled with Microsoft Visual Studio 2010 under the Windows 10 operating system. The sampling period of the control program is 10 ms. The parameters of the electro-hydraulic system are listed in Table 1.

To evaluate performances of different controllers, some indices [44] are used as follows:

$$\xi_{\max} = \max_{i=1,\cdots,N}\{|\xi_1(i)|\} \quad (66)$$

$$\xi_{average} = \frac{1}{N}\sum_{i=1}^{N}|\xi_1(i)| \quad (67)$$

$$\sigma = \sqrt{\frac{1}{N-1}\sum_{i=1}^{N}\left(|\xi_1(i)| - \xi_{average}\right)^2} \quad (68)$$

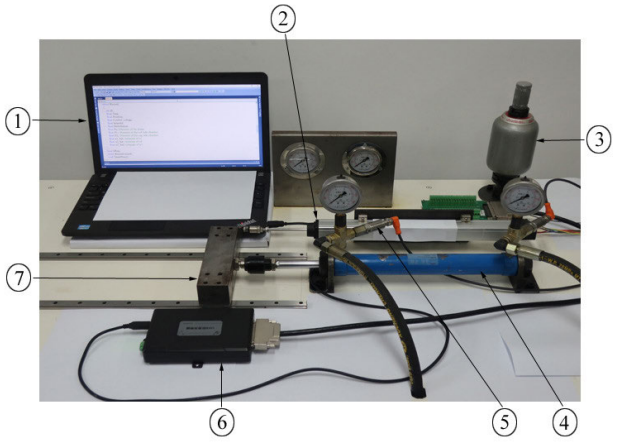

(a)

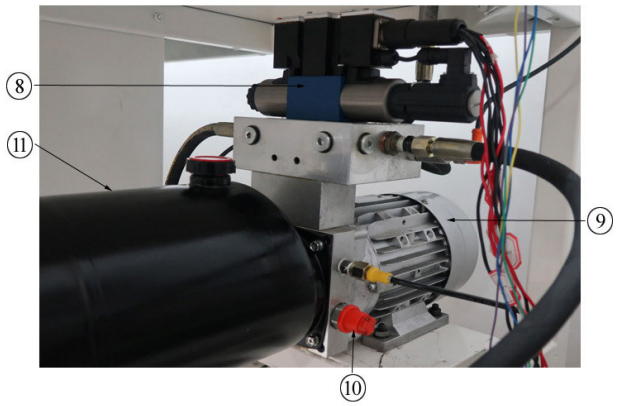

(b)

FIGURE 4. The test setup: (a) 1 – Computer, 2 – Displacement sensor, 3 – Accumulator, 4 – Cylinder, 5 – Pressure transducer, 6 – Data acquisition board, 7 – Load; (b) 8 – Proportional directional valve, 9 – Pump and electric motor, 10 – Relief valve, 11 – Oil tank.

where $\xi_1(i)$ is the tracking error at time i; $\xi_{\max}$ is the maximum of the absolute tracking error; $\xi_{average}$ is the average tracking error; N is the sample size of the tracking error; σ is the standard deviation of the tracking error.

To verify the performance of the proposed controller, we conduct four comparative experiments where four different reference trajectories are followed, respectively.

A. TRACKING THE FIRST REFERENCE TRAJECTORY

The first reference trajectory is described by

$$r = \frac{r_0(100-4t)}{(t-25)^2+4} \quad (69)$$

where $r_0 > 0$.

The external disturbance signal w_1 is given by

$$w_1(t) = \begin{cases} w_2(t), t < 8\ s \\ 0V, 8\ s \leq t < 32\ s \\ w_3(t), 32\ s \leq t < 42\ s \\ 0V, t \geq 42\ s \end{cases} \quad (70)$$

TABLE 1. Parameters of the electro-hydraulic system in experiments.

Symbol	Quantity	Value
V_{01}	initial volume of the rod side chamber	6.03×10^{-5} m^3
V_{02}	initial volume of the cap side chamber	8.04×10^{-5} m^3
A_1	ram area of the rod side	6.03×10^{-4} m^2
A_2	ram area of the cap side	8.04×10^{-4} m^2
ρ	oil density	840 kg/m^3
b	damping coefficient between piston and cylinder	5×10^3 (N·s)/m
C_{ip}	coefficient of the internal leakage of cyliner	9×10^{-13} m^5/(N·s)
g	gravitational acceleration	9.8 m/s^2
k_0	gain of the PDV	2.5×10^{-4} m/V
μ	sliding friction coefficient	0.1
m	mass of the load	3.97 kg
C_d	coefficient of discharge of the PDV orifice	0.65
β_e	effective bulk modulus of the hydraulic oil	2.7×10^8 Pa
w	area gradient of the PDV orifice	3 mm
P_S	supply pressure	5×10^6 Pa
P_T	oil tank pressure	0 Pa

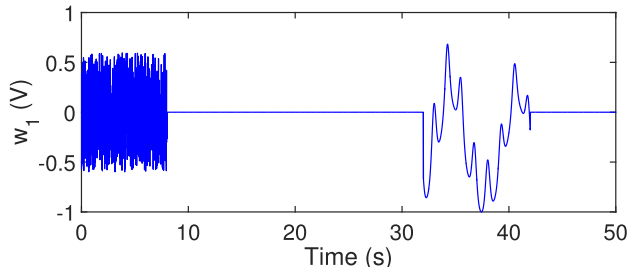

FIGURE 5. The external disturbance w_1 changes stochastically between $-0.6V$ to $0.6V$ when $t < 8s$; w_1 increases from -0.8561 V to 0.075 V during 32.29 s to 33.05 s, reduces to -0.2822 V at 33.53 s, and rises to 0.6828 V at 34.26 s.

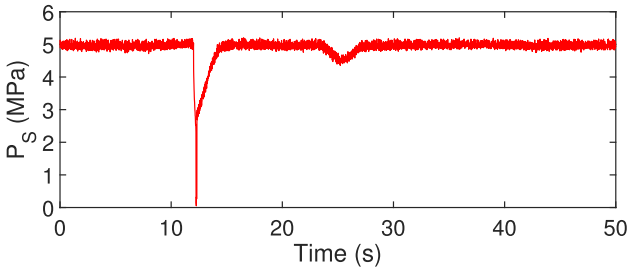

FIGURE 6. The supply pressure P_S drops steeply from 5.009 MPa to 0.0527 MPa when 11.97 s$\leq t \leq$ 12.26 s.

where $w_2(t) = rand(-0.6, 0.6)V$ and $rand(-0.6, 0.6)$ denotes the uniformly distributed random number between -0.6 and 0.6; $w_3(t) = 0.3e^{-\frac{t-32}{20}+sin(5t)} - log(2+cos(t))$ and log denotes the natural logarithm. w_1 is shown in Fig.5.

To verify the robustness of the proposed controller, the fluctuation of the supply pressure P_S is taken into account, which is described in Fig.6.

Position tracking results and performance comparison are illustrated in Fig.7 and Table 2, respectively when the first reference trajectory is followed.

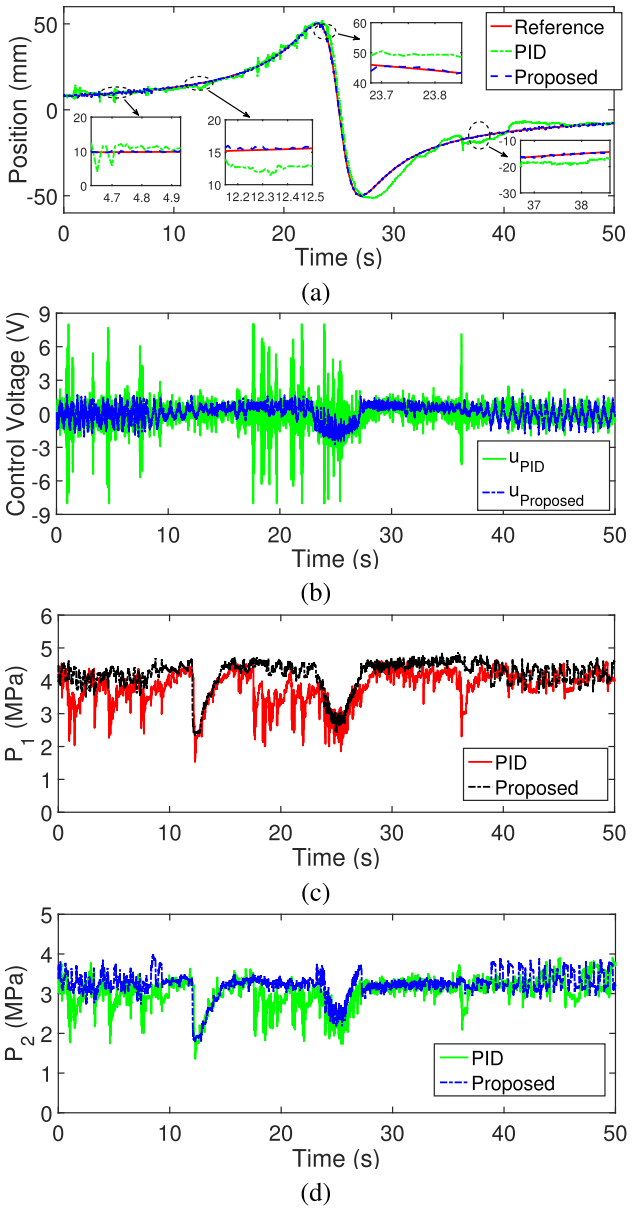

FIGURE 7. The experiment results: (a) Position, (b) Control voltage, (c) Pressure inside the rod side chamber, and (d) Pressure inside the cap side chamber when the first reference trajectory is followed.

TABLE 2. Performance comparison between the PID controler and the proposed controller when the first reference trajectory is followed in the presence of the external disturbance and the drastic supply pressure fluctuation.

Controller	$\xi_{\max}$ (mm)	$\xi_{average}$ (mm)	σ (mm)
PID	9.8485	2.1022	2.0467
Proposed	2.2627	0.3053	0.2589

The parameter of the first reference trajectory is: $r_0 = 50$ mm. The parameters of the proposed controller are: $\omega_o = 52$, $b_0 = 10$, $k_1 = 25$, $k_2 = 15.2$, $k_3 = 420$, $k_4 = 0.1$; the parameters of the PID controller are: $k_P = 108$, $k_I = 36$, $k_D = 15$. The tracking accuracy is affected by the random external disturbance. For example, in Fig.5 and

Fig.7(a), the external disturbance occurs at 4.7 s when the expected position of the load, the actual position of the load with the PID controller and that with the proposed controller are 9.758 mm, 5.806 mm, and 10.13 mm, respectively; in addition, we can observe that the external disturbance w_1 is -1 V at 37.42 s when the desired position is -15.7mm and the load moves to -15.71 mm if the EHS is adjusted by the proposed controller; by contrast, at the same time, the actual position of the load is -18.84 mm if the PID controller is used. Therefore, the load with the proposed controller can follow the desired trajectory more accurately than that with the PID controller when the external disturbance occurs. Furthermore, the drastic supply pressure variation has an effect on the tracking error of the EHS. For instance, in Fig.6 and Fig.7(a), the supply pressure drops to 0.0527 MPa at 12.26 s when the load is expected to move to 15.32 mm; at the same time, the actual positions of the load are 12.63 mm and 15.49 mm when the ESH is regulated by the PID controller and the proposed controller, respectively. Hence, the EHS regulated by the proposed controller exhibits stronger robustness than that adjusted by the PID controller when the supply pressure changes sharply. The PDV has dead-zones which give rise to the tracking lag when the expected motion direction of the load switches from left to right, or from right to left. The expected motion direction of the load is related with the sign of the tangent slope of the reference trajectory. We use k_{ref} to denote the tangent slope of the reference trajectory. From Fig.7(a), we can see that when 21.8 s$< t <$ 23 s, $k_{ref} > 0$; when 23 s$< t <$ 23.8 s, $k_{ref} < 0$. In other words, when 21.8 s$< t <$ 23 s, the load is expected to move right; when 23 s$< t <$ 23.8 s, the expected motion direction of the load switches to left. In Fig.7(a), we can observe that the desired position, the actual positions of the load with the PID controller and the proposed controller are 45.09 mm, 48.96 mm, and 45.3 mm, respectively, at 23.74 s; furthermore, when $t >$ 27 s, the expected motion direction switches to right; we can see that the load with the proposed controller can follow the reference trajectory more precisely than that with the PID controller during 27.36 s to 28.38 s. Therefore, the proposed controller shows the stronger ability to compensate for the unknown dead-zones than the PID controller.

The control voltage is described in Fig.7(b), where we use u_{PID} and $u_{Proposed}$ to denote the control voltages when the EHS is regulated by the PID controller and the proposed controller, respectively; we can observe that u_{PID} increases from -0.4006 V to 0.8739 V during 12.03 s to 12.17 s when the supply pressure varies sharply; during the same period, in order to compensate for the supply pressure fluctuation, $u_{Proposed}$ rises from 0.5833 V to 0.6802 V.

Furthermore, when 22.11 s$\leq t \leq$ 23.23 s, the desired motion direction switches from right to left, u_{PID} reduces from 0.1974 V to -1.051 V; by contrast, during the same time interval, to compensate for the dead-zones, $u_{Proposed}$ varies from 1.583 V to -1.089 V. Moreover, when 26.68 s$\leq t \leq$ 27.28 s, the expected motion direction changes from left to right, u_{PID} increases from -0.9597 V to 0.5727 V; during the same period, $u_{Proposed}$ rises from -1.328 V to 1.183 V in order that the load can follow the desired trajectory rapidly. In addition, during 0 s to 50 s, -2.7483 V$\leq u_{Proposed} \leq$ 1.8472 V such that the prescribed range of the control voltage can be satisfied; by contrast, during the same time interval, -8 V$\leq u_{PID} \leq 8$ V.

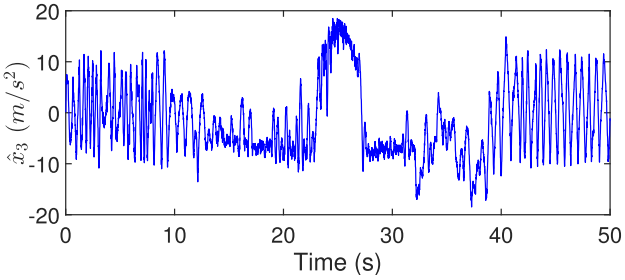

FIGURE 8. Estimate of the total disturbance when the first reference trajectory is followed; the initial values of the LESO are: $\hat{x}_1(0) = 0.3$ mm, $\hat{x}_2(0) = 0.2$ mm/s, $\hat{x}_3(0) = 0.1$ m/s^2.

The pressures of the rod side chamber and the cap side chamber are illustrated respectively in Fig.7(c) and (d), where we can observe that if the EHS is regulated by PID controller, P_1 varies from 2.899 MPa to 3.693 MPa and P_2 changes from 2.106 MPa to 2.965 MPa during 22 s to 23.15 s when the desired motion direction changes from right to left; P_1 varies from 4.494 MPa to 4.39 MPa and P_2 changes from 3.272 MPa to 3.425 MPa during the same period if the PDV is adjusted by the proposed controller. Furthermore, to compare the thrust of the cyliner under the control of two controllers, we can calculate the thrust F by (2); when the PID controller is applied, F varies from 55.01 N to -156.8 N during 22 s to 23.15 s; if the proposed controller is used, F changes from 79.17 N to -106.8 N during the same time interval such that the load moves left to track the expected trajectory instantly.

The estimate of the total disturbance is illustrated in Fig.8 when the first reference trajectory is followed and the external disturbance is described in Fig.5. We can see that in Fig.8, $\hat{x}_3$ increases from -9.637 m/s^2 to 18.49 m/s^2 during 22.83 s to 24.95 s and drops to -11.5 m/s^2 at 27.31 s; during the same time interval, P_S decreases from 4.93 MPa to 4.605 MPa and then rises to 4.969 MPa; in addition, $\hat{x}_3$ increases from -16.91 m/s^2 to 3.93 m/s^2 during 32.27 s to 34.23 s when w_1 varies from -0.8573 V to 0.6762 V. Although the real value of the total disturbance cannot be measured in the practical electro-hydraulic system regulated by the proportional directional valve, the effectiveness of the LESO can be demonstrated by the tracking accuracy of the closed-loop system because the tracking error dynamics is related with the estimation error of the total disturbance. Furthermore, we can find that the total disturbance can be estimated effectively by the LESO because the proposed controller can make the load follow the desired trajectory accurately in the presence of the external disturbance.

Moreover, in Table 2, we can see that the max absolute tracking error, the average tracking error and the standard

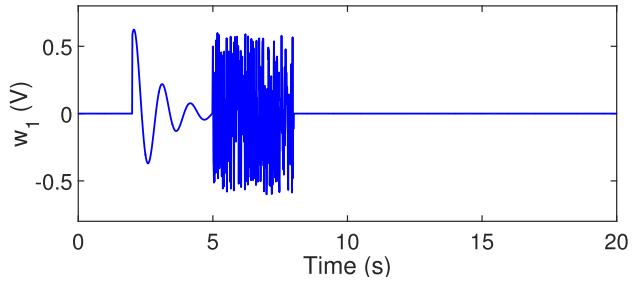

FIGURE 9. The external disturbance w_1 reduces from 0.6237 V to −0.3692V during the time interval [2.06 s, 2.6 s]; w_1 varies randomly between −0.6 V and 0.6 V when 5 s≤ t < 8 s.

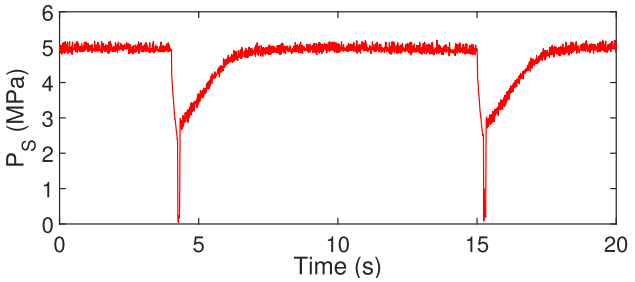

FIGURE 10. The supply pressure varies sharply at 4.27 s and 15.24 s.

deviation of the tracking error of the proposed controller are less than those of the PID controller.

B. TRACKING THE SECOND REFERENCE TRAJECTORY

The second reference trajectory is the Gaussian function, which is given by

$$r(t) = \gamma e^{-\frac{(t-\alpha)^2}{2\theta^2}} \tag{71}$$

where $\gamma > 0, \alpha > 0$, and $\theta > 0$. The disturbance signal is described by

$$w_1(t) = \begin{cases} 0\ V, 0\ s \le t < 2\ s \\ 5e^{-t}cos(6t)\ V, 2\ s \le t < 5\ s \\ w_2(t), 5\ s \le t < 8\ s \\ 0\ V, t \ge 8\ s \end{cases} \tag{72}$$

where $w_2(t) = rand(-0.6, 0.6)$ V. The external disturbance is illustrated in Fig.9.

The supply pressure is shown in Fig.10 where P_S drops from 4.951 MPa to 0.0405 MPa during 3.99 s to 4.27 s, rises to 4.808 MPa at 6.87 s, and reduces from 4.921 MPa to 0.0845 MPa when 14.98 s≤ t ≤ 15.24 s.

The position tracking results are illustrated in Fig.11 and the peformance comparison is described in Table 3 when the Gaussian function is followed.

The parameters of the reference trajectory are: $\gamma = 50$ mm, $\alpha = 10$, and $\theta = 3.6$. The parameters of the proposed controller are: $\omega_o = 50$, $b_0 = 10$, $k_1 = 20$, $k_2 = 15.2$, $k_3 = 310$, $k_4 = 0.1$; the initial values of the LESO are the same as those in Fig.7; the parameters of the PID controller are: $k_P = 270$, $k_I = 80$, $k_D = 12$. The reference

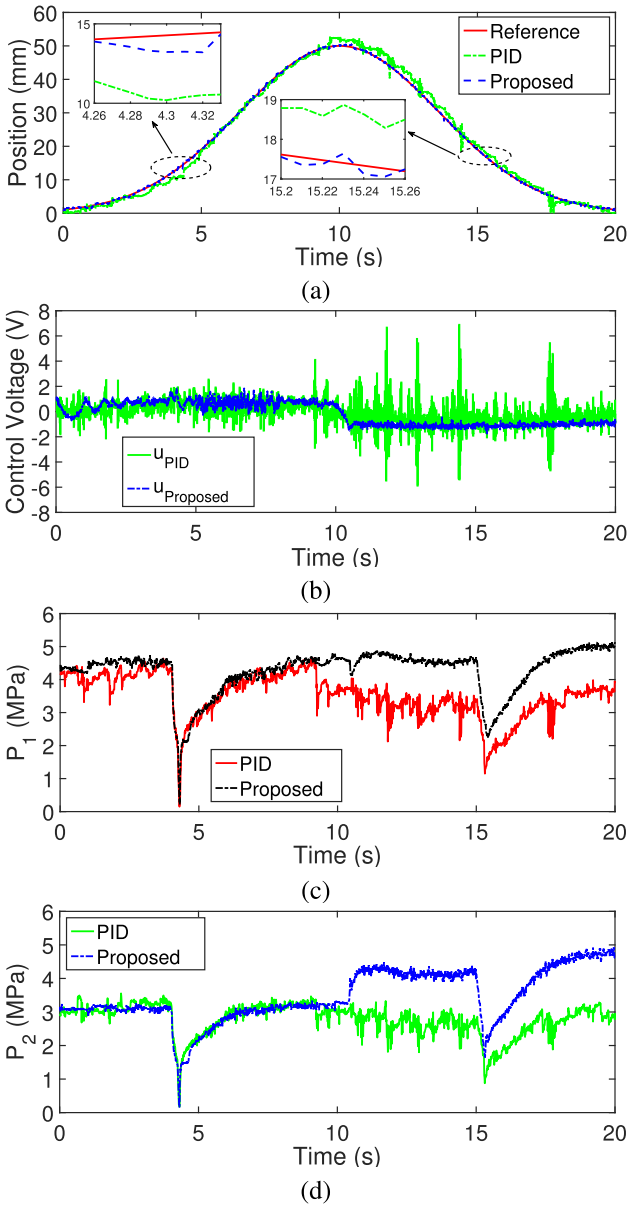

FIGURE 11. The experiment results: (a) Position, (b) Control voltage, (c) Pressure inside the rod side chamber, and (d) Pressure inside the cap side chamber when the reference trajectory is the Gaussian function.

TABLE 3. Performance comparison between the PID controler and the proposed controller when the second reference trajectory is followed.

Controller	$\xi_{\max}$ (mm)	$\xi_{average}$ (mm)	σ (mm)
PID	6.0894	1.0976	0.8264
Proposed	1.2453	0.2291	0.1870

trajectory and the actual trajectory of the load are shown in Fig.11(a), where we can observe that the expected load position, the position of the load with the PID controller, and that with the proposed controller are 14.09 mm, 11.03 mm, and 13.73 mm, respectively, when the supply pressure varies steeply at 4.27 s; the load deviates from the reference trajectory due to the disturbance when 5.06 s≤ t ≤ 5.16 s;

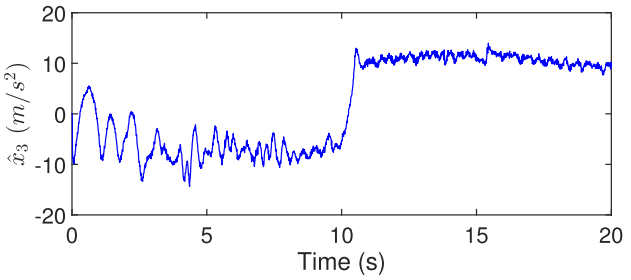

FIGURE 12. Estimate of the total disturbance when the reference trajectory is the Gaussian function.

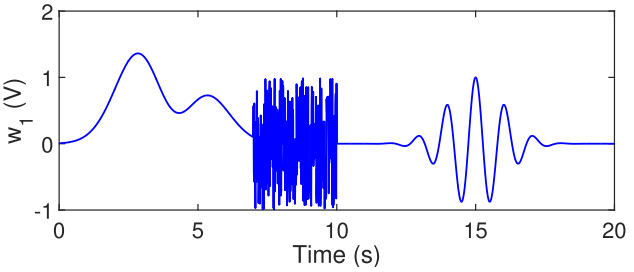

FIGURE 13. The external disturbance when the third referecne trajectory is followed.

for example, the positions of the load are 19.22 mm and 19.59 mm with the PID controller and the proposed controller, respectively, at 5.11 s when the expected position is 19.88 mm; moreover, we can see that the reference trajectory increases to the maximum at 10 s, after which the sign of the tangent slope of the reference trajectory changes. Consequently, the direction of motion of the load changes in order to track the desired trajectory. However, there exists a tracking lag due to the dead-zone in the PDV. For instance, in Fig.11(a), we can observe that the actual position of the load with the PID controller is 48.98 mm at 11.26 s when the load is expected to move left to 47.03 mm; by contrast, the load with the proposed controller moves left to 46.93 mm at the same time. Hence, the dead-zone compensation capability of the proposed controller is stronger than that of the PID controller. In addition, from Fig.11(a), we can see that the absolute tracking error of the EHS with the proposed controller is less than that with the PID controller when the supply pressure falls sharply for the second time during 15.2 s to 15.24 s.

The control voltage is illustrated in Fig.11(b), where we can see that $u_{Proposed}$ reduces from 0.9791 V to -1.517 V during 9.62 s to 10.49 s when the direction of the motion of the load changes; u_{PID} varies from -0.229 V to -1.263 V during the same period; moreover, $u_{Proposed}$ changes between -1.7519 V to 1.8500 V during 0 s to 20 s such that the prescribed voltage range is satisfied. P_1 and P_2 are described respectively in Fig. 11(c) and (d), where we can observe that P_1 reduces from 4.258 MPa to 0.182 MPa and P_2 decreases from 3.191 MPa to 0.1763 MPa if the PID controller is used when P_S changes steeply in the time interval [3.97 s, 4.31 s]; by contrast, P_1 falls from 4.51 MPa to 0.2183 MPa and P_2 reduces from 3.173 MPa to 0.1575 MPa in the same period if the proposed controller is applied. Moreover, in Fig. 11(c) and (d), if the proposed controller is used, we can calculate the thrust which reduces from 106.3 N to -176 N during 9.27 s to 10.44 s when the expected direction of the motion of the load changes; by contrast, the thrust decreases from 140.3 N to -246.9 N during the same period if the PID controller is applied.

The estimate of the total disturbance is shown in Fig.12 when the desired trajectory is the Gaussian function and the external disturbance is illustrated in Fig.9. We can see that $\hat{x}_3$ reduces from 0.2438 m/s^2 to -13.36 m/s^2 during 2.25 s to 2.62 s and increases to -2.886 m/s^2 at 3.16 s; during the same time interval, w_1 drops from 0.3135 V to -0.364 V and rises to 0.2108 V. In addition, $\hat{x}_3$ increases from -6.987 m/s^2 to 12.75 m/s^2 during 9.93 s to 10.57 s when the expected motion direction of the load switches from right to left.

Furthermore, from Table 3, we can know that the tracking performance of the proposed controller is better than that of the PID controller.

C. TRACKING THE THIRD REFERENCE TRAJECTORY

The third reference trajectory is given by

$$r(t) = r_0 \sin(\omega t + \pi) \tag{73}$$

where $r_0 > 0$, $\omega > 0$.

The external disturbance w_1 is described by

$$w_1(t) = \begin{cases} w_2(t)e^{-\frac{(t-4)^2}{2}}\ V,\ 0\ s \le t < 7\ s \\ w_3(t),\ 7\ s \le t < 10\ s \\ e^{-\frac{(t-15)^2}{2}} \cos(6(t-15))\ V,\ t \ge 10\ s \end{cases} \tag{74}$$

where $w_2(t) = 1.1(t-4)^2 - 0.55t + 2.75$, $w_3(t) = rand(-1, 1)$ V, and $rand(-1, 1)$ denotes the uniformly distributed random number between -1 and 1. w_1 is illustrated in Fig.13, where w_1 increases from 0.0586 V to 1.361 V during 0.68 s to 2.83 s, varies randomly between -1 V and 1 V during 7 s to 10 s, and rises from -0.8492 V to 0.9928 V during 14.53 s to 14.98 s.

The supply pressure P_S is described in Fig.14, where P_S drops sharply from 5.061 MPa to 0.0625 MPa during 4.01 s to 4.3 s, increases to 4.941 MPa at 7.07 s, reduces from 5.051 MPa to 0.0699 MPa during 10 s to 10.27 s, rises to 5.087 MPa at 12.87 s, and decreases from 5.249 MPa to 0.1245 MPa during 18.01 s to 18.29 s.

The parameters of the reference trajectory are: $r_0 = 50$ mm, $\omega = \pi/5$. The parameters of the proposed controller are: $\omega_o = 50$, $b_0 = 8$, $k_1 = 20$, $k_2 = 15.2$, $k_3 = 500$, $k_4 = 0.1$; the initial values of the LESO are the same as those in Fig.7; the parameters of the PID controller are: $k_P = 180$, $k_I = 120$, $k_D = 12$. The experimental results of trajectory tracking and performance comparison between two controllers are shown in Fig.15 and Table 4, respectively.

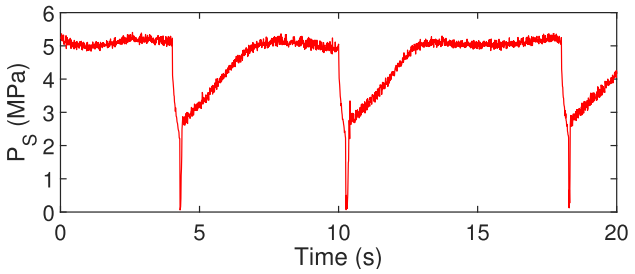

FIGURE 14. The supply pressure changes steeply when 4.01 s$\leq t \leq$ 4.3 s, 10 s$\leq t \leq$ 10.27 s, and 18.01 s$\leq t \leq$ 18.29 s.

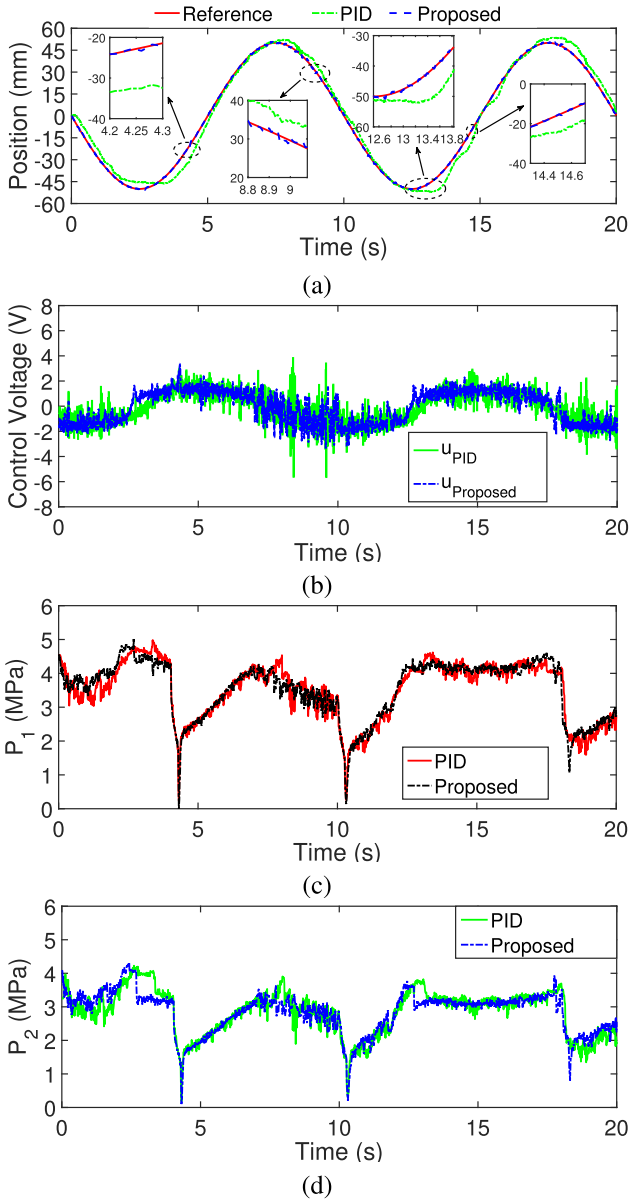

FIGURE 15. The experimental results: (a) Position, (b) Control voltage, (c) Pressure inside the rod side chamber, and (d) Pressure inside the cap side chamber when the third reference trajectory is followed and the supply pressure varies.

In Fig.15(a), we can see that the desired position, the position of the load with the PID controller and that with the proposed controller are −21.42 mm, −32.46 mm and −22.44 mm, respectively, when the supply pressure P_S reduces to 0.0625 MPa at 4.3 s. In addition, if the proposed controller is applied, the load moves to 30.39 mm at 9 s when the expected position is 29.57 mm and the random external disturbance occurs; if the PID controller is used, the load moves to 34.89 mm at the same time. The dead-zone of the proportional directional valve results in the tracking lag when the sign of the tangent slope of the reference trajectory varies. For example, in Fig.15(a), we can see the effect of the dead-zone on the control performance by observing that there is a tracking lag during 12.82 s to 13.35 s when the sign of the tangent slope of the desired trajectory switches to positive and the PID controller is utilized; by contrast, the load can follow the reference trajectory rapidly in the same time interval if the proposed controller is used. Furthermore, we can find that the load is expected to move right to −45.23 mm at 13.21 s when the actual positions of the load with the PID controller and the proposed controller are −52.02 mm and −45.35 mm, respectively.

The control voltage is illustrated in Fig.15(b), where we can observe that −5.6391 V$\leq u_{PID} \leq$ 3.8337 V; by contrast, −3.3432 V$\leq u_{Proposed} \leq$ 3.3764 V such that the prescribed voltage range can be satisfied. The pressures of two chambers are described respectively in Fig.15(c) and (d), where we can see that if the PID controller is used, P_1 reduces from 3.298 MPa to 0.2603 MPa and P_2 decreases from 2.709 MPa to 0.308 MPa during 10 s to 10.31 s when the supply pressure drops sharply; P_1 reduces from 3.181 MPa to 0.1604 MPa and P_2 decreases from 2.664 MPa to 0.2044 MPa during the same period if the proposed controller is applied.

Estimate of the total disturbance is shown in Fig.16 when the third reference trajectory is followed and the external disturbance is described in Fig.13. We can observe that $\hat{x}_3$ decreases from −1.906 m/s^2 to −18 m/s^2 during 13.98 s to 14.57 s, rises to 0.4489 m/s^2 at 15.03 s and reduces to −17.13 m/s^2 at 15.49 s in Fig.16.

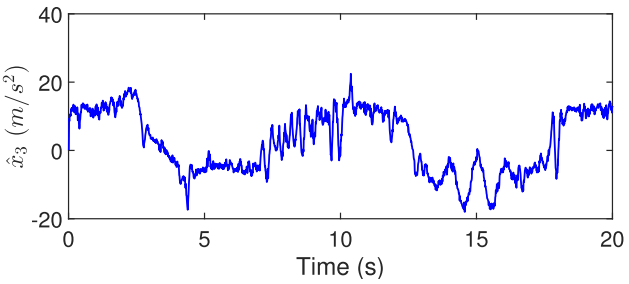

FIGURE 16. Estimate of the total disturbance when the third reference trajectory is followed.

TABLE 4. Performance comparison between the PID controler and the proposed controller when the third reference trajectory is followed.

Controller	$\xi_{\max}$ (mm)	$\xi_{average}$ (mm)	σ (mm)
PID	11.3471	3.7463	2.4411
Proposed	2.5972	0.3526	0.3419

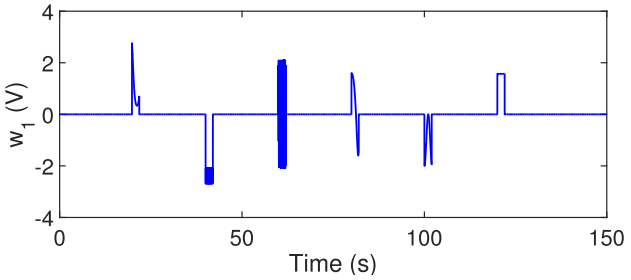

FIGURE 17. The external disturbance when the fourth reference trajectory is followed.

Moreover, from Table 4, we can see that performance indices of the proposed controller are less than those of the PID controller. As a result, the EHS regulated by the proposed controller can follow the expected trajectory more precisely than that adjusted by the PID controller.

D. TRACKING THE FOURTH REFERENCE TRAJECTORY

The fourth reference trajectory is given by

$$r(t) = r_0(a_1 cos(\omega t - \frac{\pi}{2}) + a_2 cos(3\omega t - \frac{\pi}{2})) \quad (75)$$

where $r_0 > 0, a_1 > 0, a_2 > 0, \omega > 0$.

The external disturbance w_1 is described by

$$w_1(t) = \begin{cases} 0\ V,\ t < 19.83\ s \\ 3^{sin(2t)}\ V,\ 19.83\ s \le t < 21.83\ s \\ 0\ V,\ 21.83\ s \le t < 40\ s \\ w_2(t),\ 40\ s \le t < 42\ s \\ 0\ V,\ 42\ s \le t < 60\ s \\ w_3(t),\ 60\ s \le t < 62\ s \\ 0\ V,\ 62\ s \le t < 80\ s \\ w_4(t),\ 80\ s \le t < 82\ s \\ 0\ V,\ 82\ s \le t < 100\ s \\ w_5(t),\ 100\ s \le t < 102\ s \\ 0\ V,\ 102\ s \le t < 120\ s \\ w_6(t),\ 120\ s \le t < 122\ s \\ 0\ V,\ t \ge 122\ s \end{cases} \quad (76)$$

where $w_2(t) = -1.5log(5 + cos(t^2))$ V, $w_3(t) = 2.1sin(cosh(t))$ V, $w_4(t) = 1.6cos(sinh(t - 80))$ V, $w_5(t) = sin(3t) - sin(\sqrt{2}t)$ V, and $w_6(t) = arctan(cosh(8t) - 10t)$ V. w_1 is illustrated in Fig.17, where w_1 reduces from 2.738 V to 0.3333 V during 19.84 s to 21.21 s and decreases from 1.571 V to 0 V during 120.5 s to 122.1 s.

The parameters of the reference trajectory are: $r_0 = 42$ mm, $a_1 = \frac{4}{\pi}$, $a_2 = \frac{4}{3\pi}$, $\omega = \frac{\pi}{20}$. The parameters of the proposed controller are: $\omega_o = 50$, $b_0 = 8$, $k_1 = 20$, $k_2 = 15.2$, $k_3 = 500$, $k_4 = 0.1$; the initial values of the LESO are: $\hat{x}_1(0) = 0.1$ mm, $\hat{x}_2(0) = 9.2$ mm/s, $\hat{x}_3(0) = 9.1981$ m/s^2; the parameters of the PID controller are: $k_P = 180$, $k_I = 120$, $k_D = 12$. The experimental results of trajectory tracking

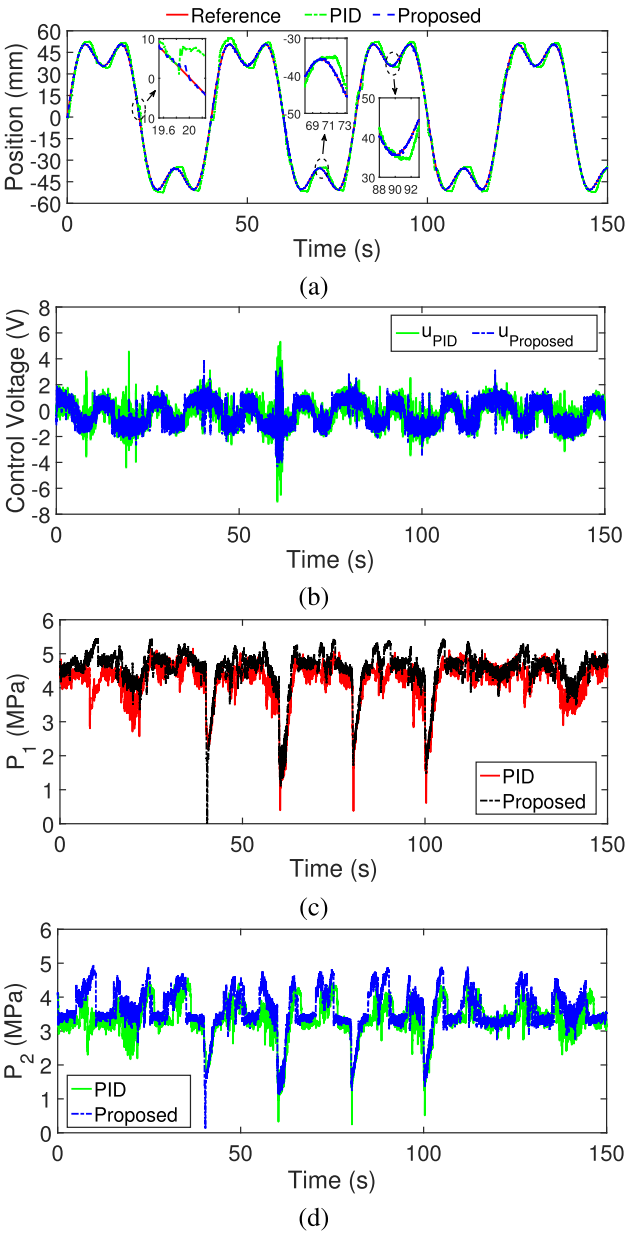

FIGURE 18. The experimental results: (a) Position, (b) Control voltage, (c) Pressure inside the rod side chamber, and (d) Pressure inside the cap side chamber when the fourth reference trajectory is followed.

TABLE 5. Performance comparison between the PID controller and the proposed controller when the fourth reference trajectory is followed.

Controller	ξ_{max} (mm)	$\xi_{average}$ (mm)	σ (mm)
PID	11.7687	2.3303	1.7985
Proposed	2.8832	0.2553	0.2685

and performance comparison between two controllers are described in Fig.18 and Table 5, respectively.

The effects of dead-zone can be observed when the expected motion direction changes. Therefore, to distinguish the effect caused by the dead-zone from that caused by the external disturbance, we let the external disturbance occur in the time interval in which the expected motion direction keeps unchanged. For example, during 19.85 s to 20.13 s, the sign

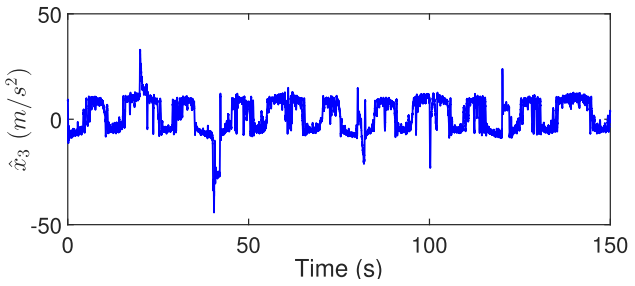

FIGURE 19. Estimate of the total disturbance when the fourth reference trajectory is followed.

of the tangent slope of the reference trajectory keeps negative; hence, the tracking error during this period is brought about mainly by the external disturbance which varies from 2.713 V to 1.826 V in the same time interval. Moreover, from Fig.18(a), we can find that the proposed controller can make the load follow the reference trajectory more precisely than the PID controller during 19.85 s to 20.13 s when the external disturbance exists.

The ability for dead-zone compensation is shown in Fig.18(a) when the sign of the tangent slope of the reference trajectory switches. For example, there is no occurrence of the external disturbance during 68.22 s to 73.23 s when the expected motion direction of the load switches from right to left. In this case, the tracking lag occurs due to the dead-zone of the proportional directional valve. It is evident that there is a large tracking lag during 70.75 s to 71.71 s if the PID controller is utilized, whereas the load can follow the reference trajectory immediately if the proposed controller is used.

The control voltage, the pressure of rod side chamber, the pressure of cap side chamber, and the estimate for the total disturbance are demonstrated in Fig.18(b), (c), (d) and Fig.19, respectively. From Fig.19, we can see that $\hat{x}_3$ varies between -44.25 m/s^2 and 32.94 m/s^2 during 0 s to 150 s. Furthermore, we can find that the total disturbance can be estimated effectively by the LESO since the load can follow the reference trajectory exactly under the control of the proposed controller when the external disturbance occurs.

Hence, from the results of the fourth experiment for trajectory tracking, we can find that the proposed controller has stronger abilities in both disturbance rejection and dead-zone compensation than the PID controller.

VI. CONCLUSION

We focus on the practical EHS regulated by the PDV, whose dead-zones are unknown and difficult to measure; furthermore, the random external disturbance and the supply pressure variation occur when the electro-hydraulic system works; moreover, the control voltage is required to satisfy the prescribed voltage range. Hence, it is difficult to design the controller for the electro-hydraulic system regulated by the PDV. Fortunately, the dead-zones, the random external disturbance, and the supply pressure fluctuation can be viewed as a total disturbance which can be estimated by the LESO; furthermore, a novel disturbance rejection controller is put forward to compensate for the total disturbance such that the load can follow the reference trajectory precisely and the control voltage is restricted to protect the PDV from being damaged. Stability of the EHS is analyzed in detail to ensure that the tracking error ultimately stays within the arbitrarily small neighborhood of the origin. Comparative experimental results demonstrate that the proposed controller outperforms the PID controller in terms of both dead-zones compensation and disturbance rejection when the supply pressure fluctuates sharply.

The reference signals involved in the article can be taken the second derivatives with respect to time, but in the practical engineering, there are non-smooth reference signals whose second derivatives do not exist. In the future work, we will improve the controller so that the non-smooth reference signal can be followed.

REFERENCES

[1] S.-H. Hyon, D. Suewaka, Y. Torii, and N. Oku, "Design and experimental evaluation of a fast torque-controlled hydraulic humanoid robot," *IEEE/ASME Trans. Mechatronics*, vol. 22, no. 2, pp. 623–634, Apr. 2017, doi: 10.1109/TMECH.2016.2628870.

[2] Y. Li and Q. Wang, "Adaptive neural finite-time trajectory tracking control of hydraulic excavators," *Proc. Inst. Mech. Eng. I, J. Syst. Control Eng.*, vol. 232, no. 7, pp. 909–925, Aug. 2018, doi: 10.1177/0959651818767770.

[3] J. Zhao, J. Wang, and S. Wang, "Fractional order control to the electro-hydraulic system in insulator fatigue test device," *Mechatronics*, vol. 23, no. 7, pp. 828–839, Oct. 2013, doi: 10.1016/j.mechatronics.2013.02.002.

[4] C. Wang, Z. Jiao, and L. Quan, "Adaptive velocity synchronization compound control of electro-hydraulic load simulator," *Aerosp. Sci. Technol.*, vol. 42, pp. 309–321, Apr. 2015, doi: 10.1016/j.ast.2015.01.018.

[5] G. Shen, Z.-C. Zhu, X. Li, Y. Tang, D.-D. Hou, and W.-X. Teng, "Real-time electro-hydraulic hybrid system for structural testing subjected to vibration and force loading," *Mechatronics*, vol. 33, pp. 49–70, Feb. 2016, doi: 10.1016/j.mechatronics.2015.10.009.

[6] B. Eryilmaz and B. H. Wilson, "Unified modeling and analysis of a proportional valve," *J. Franklin Inst.*, vol. 343, no. 1, pp. 48–68, Jan. 2006, doi: 10.1016/j.jfranklin.2005.07.001.

[7] G. M. Wu, M. X. Qiu, and Q. F. Wang, *Electrohydraulic Proportional Technique in Theory and Application*. Hangzhou, China: Zhejiang Univ. Press, 2006.

[8] B. Xu, Q. Su, J. Zhang, and Z. Lu, "Analysis and compensation for the cascade dead-zones in the proportional control valve," *ISA Trans.*, vol. 66, pp. 393–403, Jan. 2017, doi: 10.1016/j.isatra.2016.10.012.

[9] A. Mohanty and B. Yao, "Integrated direct/indirect adaptive robust control of hydraulic manipulators with valve deadband," *IEEE/ASME Trans. Mechatronics*, vol. 16, no. 4, pp. 707–715, Aug. 2011, doi: 10.1109/TMECH.2010.2051037.

[10] I.-Y. Lee, D.-H. Oh, S.-W. Ji, and S.-N. Yun, "Control of an overlap-type proportional directional control valve using input shaping filter," *Mechatronics*, vol. 29, pp. 87–95, Aug. 2015, doi: 10.1016/j.mechatronics.2014.10.003.

[11] S. Liu and B. Yao, "Characterization and attenuation of sandwiched deadband problem using describing function analysis and application to electrohydraulic systems controlled by closed-center valves," *J. Dyn. Syst., Meas., Control*, vol. 131, no. 3, May 2009, Art. no. 031002, doi: 10.1115/1.3089557.

[12] F. Bu and B. Yao, "Nonlinear adaptive robust control of hydraulic actuators regulated by proportional directional control valves with deadband and nonlinear flow gains," in *Proc. Amer. Control Conf. (ACC)*, Chicago, IL, USA, 2000, pp. 4129–4133.

[13] Z. Zhang, J. H. Park, K. Zhang, and J. Lu, "Adaptive control for a class of nonlinear time-delay systems with dead-zone input," *J. Franklin Inst.*, vol. 353, no. 17, pp. 4400–4421, Nov. 2016, doi: 10.1016/j.jfranklin.2016.08.014.

[14] W. Deng, J. Yao, and D. Ma, "Robust adaptive precision motion control of hydraulic actuators with valve dead-zone compensation," *ISA Trans.*, vol. 70, pp. 269–278, Sep. 2017, doi: 10.1016/j.isatra.2017.07.022.

[15] R. Sakthivel, P. Selvaraj, K. Mathiyalagan, and J. H. Park, "Robust fault-tolerant H_∞ control for offshore steel jacket platforms via sampled-data approach," *J. Franklin Inst.*, vol. 352, no. 6, pp. 2259–2279, Jun. 2015, doi: 10.1016/j.jfranklin.2015.03.016.

[16] Q. Guo, X. Li, and D. Jiang, "Full-state error constraints based dynamic surface control of electro-hydraulic system," *IEEE Access*, vol. 6, pp. 53092–53101, 2018, doi: 10.1109/ACCESS.2018.2870956.

[17] C. Sun, J. Fang, J. Wei, and B. Hu, "Nonlinear motion control of a hydraulic press based on an extended disturbance observer," *IEEE Access*, vol. 6, pp. 18502–18510, 2018, doi: 10.1109/ACCESS.2018.2813317.

[18] H. Angue Mintsa, R. Venugopal, J.-P. Kenne, and C. Belleau, "Feedback linearization-based position control of an electrohydraulic servo system with supply pressure uncertainty," *IEEE Trans. Control Syst. Technol.*, vol. 20, no. 4, pp. 1092–1099, Jul. 2012, doi: 10.1109/TCST.2011.2158101.

[19] H. E. Merritt, *Hydraulic Control Systems*. New York, NY, USA: Wiley, 1967.

[20] G. Yang, J. Yao, G. Le, and D. Ma, "Adaptive integral robust control of hydraulic systems with asymptotic tracking," *Mechatronics*, vol. 40, pp. 78–86, Dec. 2016, doi: 10.1016/j.mechatronics.2016.10.007.

[21] Q. Guo, J. Yin, T. Yu, and D. Jiang, "Saturated adaptive control of an electrohydraulic actuator with parametric uncertainty and load disturbance," *IEEE Trans. Ind. Electron.*, vol. 64, no. 10, pp. 7930–7941, Oct. 2017, doi: 10.1109/TIE.2017.2694352.

[22] S. Duraiswamy and G. T.-C. Chiu, "Nonlinear adaptive nonsmooth dynamic surface control of electro-hydraulic systems," in *Proc. Amer. Control Conf.*, Denver, CO, USA, 2003, pp. 3287–3292.

[23] J. Yao, W. Deng, and Z. Jiao, "Adaptive control of hydraulic actuators with LuGre model-based friction compensation," *IEEE Trans. Ind. Electron.*, vol. 62, no. 10, pp. 6469–6477, Oct. 2015, doi: 10.1109/TIE.2015.2423660.

[24] B. Yao, F. Bu, J. Reedy, and G. T.-C. Chiu, "Adaptive robust motion control of single-rod hydraulic actuators: Theory and experiments," *IEEE/ASME Trans. Mechatronics*, vol. 5, no. 1, pp. 79–91, Mar. 2000, doi: 10.1109/3516.828592.

[25] W. Kim, D. Shin, D. Won, and C. C. Chung, "Disturbance-observer-based position tracking controller in the presence of biased sinusoidal disturbance for electrohydraulic actuators," *IEEE Trans. Control Syst. Technol.*, vol. 21, no. 6, pp. 2290–2298, Nov. 2013, doi: 10.1109/TCST.2013.2237909.

[26] D. Won, W. Kim, D. Shin, and C. C. Chung, "High-gain disturbance observer-based backstepping control with output tracking error constraint for electro-hydraulic systems," *IEEE Trans. Control Syst. Technol.*, vol. 23, no. 2, pp. 787–795, Mar. 2015, doi: 10.1109/TCST.2014.2325895.

[27] R. Sakthivel, S. Mohanapriya, C. K. Ahn, and P. Selvaraj, "State estimation and dissipative-based control design for vehicle lateral dynamics with probabilistic faults," *IEEE Trans. Ind. Electron.*, vol. 65, no. 9, pp. 7193–7201, Sep. 2018, doi: 10.1109/TIE.2018.2793253.

[28] J. Liu, *Robot Control System Design and MATLAB Simulation: The Advanced Design Method*. Beijing, China: Tsinghua Univ. Press, 2017.

[29] A. Ailon, "Simple tracking controllers for autonomous VTOL aircraft with bounded inputs," *IEEE Trans. Autom. Control*, vol. 55, no. 3, pp. 737–743, Mar. 2010, doi: 10.1109/TAC.2010.2040493.

[30] C. Wen, J. Zhou, Z. Liu, and H. Su, "Robust adaptive control of uncertain nonlinear systems in the presence of input saturation and external disturbance," *IEEE Trans. Autom. Control*, vol. 56, no. 7, pp. 1672–1678, Jul. 2011, doi: 10.1109/TAC.2011.2122730.

[31] K. Baghestan, S. M. Rezaei, H. A. Talebi, and M. Zareinejad, "An energy-saving nonlinear position control strategy for electro-hydraulic servo systems," *ISA Trans.*, vol. 59, pp. 268–279, Nov. 2015, doi: 10.1016/j.isatra.2015.10.012.

[32] R. Mao, "Research on the nonlinearity and control method for the proportional valve controlled hydraulic cylinder system," M.S. thesis, Sch. Autom., Beijing Inst. Technol., Beijing, China, 2015.

[33] J. Han, "Extended state observer for a class of uncertain plants," *Control Decis.*, vol. 10, no. 1, pp. 85–88, 1995.

[34] J. Han, "Auto-disturbances-rejection controller and its applications," *Control Decis.*, vol. 13, no. 1, pp. 19–23, 1998.

[35] J. Han, "From PID to active disturbance rejection control," *IEEE Trans. Ind. Electron.*, vol. 56, no. 3, pp. 900–906, Mar. 2009, doi: 10.1109/TIE.2008.2011621.

[36] Z. Chen, Y. Li, Z. Yuan, M. Sun, Z. Liu, and Q. Sun, "Attitude control of tandem rotor helicopter based on cascade active disturbance rejection control," *Control Theory Appl.*, vol. 32, no. 9, pp. 1219–1225, 2015.

[37] J. Tao, Q. Sun, Z. Chen, and Y. He, "Homing control of a parafoil system in large wind environments," *Control Appl.*, vol. 33, no. 12, pp. 1630–1638, 2016.

[38] W. Xue and Y. Huang, "Performance analysis of 2-DOF tracking control for a class of nonlinear uncertain systems with discontinuous disturbances," *Int. J. Robust Nonlinear Control*, vol. 28, no. 4, pp. 1456–1473, Mar. 2018, doi: 10.1002/rnc.3972.

[39] Z. Gao, "Scaling and bandwidth-parameterization based controller tuning," in *Proc. Amer. Control Conf.*, Denver, CO, USA, 2003, pp. 4989–4996.

[40] W. Deng and J. Yao, "Extended-state-observer-based adaptive control of electro-hydraulic servomechanisms without velocity measurement," *IEEE/ASME Trans. Mechatronics*, early access, Dec. 12, 2019, doi: 10.1109/TMECH.2019.2959297.

[41] W. Deng, J. Yao, and D. Ma, "Time-varying input delay compensation for nonlinear systems with additive disturbance: An output feedback approach," *Int. J. Robust Nonlinear Control*, vol. 28, no. 1, pp. 31–52, Jan. 2018, doi: 10.1002/rnc.3853.

[42] H. K. Khalil, *Nonlinear System* 3rd ed. Upper Saddle River, NJ, USA: Prentice-Hall, 2002.

[43] Q. Zheng, L. Dong, D. H. Lee, and Z. Gao, "Active disturbance rejection control for MEMS gyroscopes," *IEEE Trans. Control Syst. Technol.*, vol. 17, no. 6, pp. 1432–1438, Nov. 2009, doi: 10.1109/TCST.2008.2008638.

[44] G. Yang, J. Yao, G. Le, and D. Ma, "Asymptotic output tracking control of electro-hydraulic systems with unmatched disturbances," *IET Control Theory Appl.*, vol. 10, no. 18, pp. 2543–2551, Dec. 2016, doi: 10.1049/iet-cta.2016.0702.

SHENGFEI LIU received the M.E. degree in computer science from Nankai University, Tianjin, China, in 2004, where he is currently pursuing the Ph.D. degree in control science and engineering with the College of Artificial Intelligence.

His research interests include nonlinear optimization, embedded control systems, robust control, adaptive control, and disturbance rejection control with applications to the electro-hydraulic systems.

LIWU WANG received the M.E. degree in aeronautical engineering from Northwestern Polytechnical University, Xi'an, China, in 2013. He is currently pursuing the Ph.D. degree in civil engineering with Southeast University, Nanjing, China. He is also with the Beijing Institute of Space Mechanics and Electricity.

His research interests include recovery and landing of spacecraft and space flexible deployable aerodynamic decelerator.

CHUN LI received the M.E. degree in aircraft design from the China Academy of Space Technology, Beijing, China, in 2006.

She is currently with the Beijing Institute of Space Mechanics and Electricity. Her research interests include spacecraft electronics and automatic control.

QINGLIN SUN received the B.E. and M.E. degrees in control theory and control engineering from Tianjin University, Tianjin, China, in 1985 and 1990, respectively, and the Ph.D. degree in control science and engineering from Nankai University, Tianjin, in 2003.

He is currently a Professor with the College of Artificial Intelligence, Nankai University. He has published more than 100 peer-reviewed articles. His research interests include self-adaptive control, modeling and control of flexible spacecraft, complex systems, and embedded control systems and their applications.

ZENGQIANG CHEN received the B.S. degree in mathematics and the M.S. and Ph.D. degrees in control theory and control engineering from Nankai University, Tianjin, China, in 1987, 1990, and 1997, respectively.

Since 1990, he has been with Nankai University, where he is currently a Professor with the College of Artificial Intelligence. He has authored or coauthored more than 200 journal articles. His main research interests include adaptive control, predictive control, intelligent control, and nonlinear control.

MINGWEI SUN received the Ph.D. degree from the Department of Computer and Systems Science, Nankai University, Tianjin, China, in 2000.

From 2000 to 2008, he was a Flight Control Engineer with the Beijing Electro-Mechanical Engineering Research Institute, Beijing, China. Since 2009, he has been with Nankai University, where he is currently a Professor with the College of Artificial Intelligence. His research interests include flight control, guidance, model predictive control, active disturbance rejection control, and nonlinear optimization.

XIANYI ZENG (Senior Member, IEEE) received the B.Eng. degree from Tsinghua University, Beijing, China, in 1986, and the Ph.D. degree from the Centre d'Automatique, Université des Sciences et Technologies de Lille, Villeneuve-d'Ascq, France, in 1992.

He is currently a Professor with the Ecole Nationale Supérieure des Arts et Industries Textiles, Roubaix, France. His research interests include intelligent decision support systems for fashion and material design and modeling and analysis of human perception and cognition on industrial products and their integration into virtual products.